General Disclaimer

One or more of the Following Statements may affect this Document

- This document has been reproduced from the best copy furnished by the organizational source. It is being released in the interest of making available as much information as possible.

- This document may contain data, which exceeds the sheet parameters. It was furnished in this condition by the organizational source and is the best copy available.

- This document may contain tone-on-tone or color graphs, charts and/or pictures, which have been reproduced in black and white.

- This document is paginated as submitted by the original source.

- Portions of this document are not fully legible due to the historical nature of some of the material. However, it is the best reproduction available from the original submission.

NASA TECHNICAL MEMORANDUM

NASA TM X-72761

NASA TM X-72761

LOW-SPEED WIND TUNNEL INVESTIGATION OF A LARGE-SCALE ADVANCED ARROW WING SUPERSONIC TRANSPORT CONFIGURATION WITH ENGINES MOUNTED ABOVE THE WING FOR UPPER-SURFACE BLOWING

By

James P. Shivers, H. Clyde McLemore

and

Paul L. Coe, Jr.

" Publicly Released August 2, 1977 "

NATIONAL AERONAUTICS AND SPACE ADMINISTRATION
LANGLEY RESEARCH CENTER, HAMPTON, VIRGINIA 23665

1. Report No.	2. Government Accession No.	3. Recipient's Catalog No.
TM X-72761		

4. Title and Subtitle	5. Report Date
LOW-SPEED WIND TUNNEL INVESTIGATION OF A LARGE-SCALE ADVANCED ARROW WING SUPERSONIC TRANSPORT CONFIGURATION WITH ENGINES MOUNTED ABOVE THE WING FOR UPPER-SURFACE BLOWING	August 1975
	6. Performing Organization Code

7. Author(s)	8. Performing Organization Report No.
James P. Shivers, H. Clyde McLemore and Paul L. Coe, Jr.	

9. Performing Organization Name and Address	10. Work Unit No.
NASA Langley Research Center Hampton, VA 23665	743-04-12-02
	11. Contract or Grant No.
	13. Type of Report and Period Covered
12. Sponsoring Agency Name and Address	Technical Memorandum
National Aeronautics and Space Administration Washington, DC 20546	14. Sponsoring Agency Code

15. Supplementary Notes

16. Abstract

Tests have been conducted in the Langley full-scale tunnel to determine the low-speed aerodynamic characteristics of a large-scale advanced arrow-wing supersonic transport configuration with engines mounted above the wing for upper-surface blowing. Tests were made over an angle-of-attack range of -10° to 32°, sideslip angles of $\pm 5^{\circ}$, and a Reynolds number range of 3.53×10^{6} to 7.33×10^{6} (referenced to mean aerodynamic chord of the wing). Configuration variables included trailing-edge flap deflection, engine jet nozzle angle, engine thrust coefficient, engine out operation, and asymmetrical trailing-edge BLC for providing roll trim. Downwash measurements at the tail were obtained for different thrust coefficients, tail heights, and at two fuselage stations.

17. Key Words (Suggested by Author(s)) (STAR category underlined)	18. Distribution Statement
Aerodynamics, Low Speed Stability and Control, Advanced Supersonic Transport	

19. Security Classif. (of this report)	20. Security Classif. (of this page)	21. No. of Pages	22. Price*
Unclassified	Unclassified	67	$4.25

LOW-SPEED WIND TUNNEL INVESTIGATION OF A LARGE-SCALE ADVANCED ARROW WING SUPERSONIC TRANSPORT CONFIGURATION WITH ENGINES MOUNTED ABOVE THE WING FOR UPPER-SURFACE BLOWING

James P. Shivers, H. Clyde McLemore

and

Paul L. Coe, Jr.

Langley Research Center
Hampton, Virginia

SUMMARY

Tests have been conducted in the Langley full-scale tunnel to determine the low-speed aerodynamic characteristics of a large-scale advanced arrow-wing supersonic transport configuration with engines mounted above the wing for upper-surface blowing.

The results of the investigation indicated that the use of upper-surface blowing was effective for providing the high lift required for improved take-off and landing performance. Although large diving moments accompanied the high propulsive lift, analysis indicated that an all-movable, retractable canard in combination with a relatively small conventional tail may be an effective arrangement for achieving low-speed longitudinal stability and trim. The model exhibited static directional stability up to an angle of attack of about 20° and had high positive effective dihedral. Large rolling and yawing moments were introduced with one engine inoperative; however the use of

asymmetric boundary-layer control (BLC) on the trailing-edge flaps appeared to be one method of providing engine-out roll and yaw trim. Spoiler deflection provided relatively large lateral control moments.

INTRODUCTION

The present investigation was conducted to determine the low-speed performance and stability and control characteristics of an advanced arrow-wing supersonic transport configuration with engines mounted above the wing for upper-surface blowing (USB). The investigation was made as part of a general research program to provide a technology base for the formulation and development of an advanced supersonic transport configuration. Other investigations conducted as part of this program are reported in references 1 and 2.

Although the highly swept arrow-wing supersonic transport configuration is expected to be aerodynamically efficient at high speeds (see refs. 3 and 4), past configurations of this type have embodied several design features which result in poor take-off and landing performance. For example, the trailing-edge flaps were relatively ineffective because the conventional lower surface engine arrangement occupied most of the inboard wing span and the flaps were therefore limited to small spanwise segments between the engines. The small flap segments and a relatively long fuselage, which restricted the ground rotation angle to 10° or less, resulted in maximum values of take-off and landing lift coefficients of only about 0.5. Because of the low values of lift coefficient, a wing area somewhat greater than that required for efficient cruise performance must be used in order to provide acceptable take-off and landing speeds and runway lengths. One means of providing additional lift with a wing sized for efficient cruise is the use of the USB concept. In the

USB concept, the engines, or possible the inboard engines only, are located above the wing such that the exhaust flow can be deflected over the trailing-edge flaps. In such an arrangement, the trailing-edge flap span can be made continuous in order to achieve the maximum lift effectiveness provided by USB.

The present investigation consisted of low-speed wind tunnel tests to determine the performance and static stability and control characteristics of a large-scale model of an advanced arrow-wing supersonic transport configuration having engines mounted on top of the wing for USB. The tests were conducted in the Langley full-scale tunnel for a range of Reynolds number from 3.53×10^6 to 7.33×10^6 (corresponding to test velocities of about 30.08 Kts (50.8 ft/sec) and 62.05 Kts (104.8 ft/sec), respectively. The tests were conducted for a range of angles of attack from about -10° to 32° and sideslip angles of $\pm 5^\circ$. The configuration variables included trailing-edge flap deflection, engine jet nozzle angle, and engine thrust coefficient. Also included in the investigation were tests to measure the forces and moments produced in the one-engine inoperative condition. Tests were also conducted to examine the use of asymmetrical trailing-edge BLC for providing roll trim in the one-engine inoperative condition.

SYMBOLS

The longitudinal data are referred to the wind system of axes and the lateral-directional data are referred to the body system of axes illustrated in figure 1. The moment reference center for the tests was 53.8-percent of the wing mean aerodynamic chord.

The dimensional quantities herein are given both in the International System of Units (SI), and in U. S. Customary Units.

b	wing span, 4.191 m (13.750 ft)
B. S.	body station (longitudinal distance from model nose, m (ft)
$\bar{c}$	mean aerodynamic chord, 3.368m (11.050 ft)
C_D	drag coefficient, Drag/qS
C_L	lift coefficient, Lift/qS
C_{L_Γ}	circulation lift
C_ℓ	rolling-moment coefficient, $\frac{\text{Rolling moment}}{qSb}$
C_m	pitching-moment coefficient, $\frac{\text{Pitching moment}}{qS\bar{c}}$
C_n	yawing-moment coefficient, $\frac{\text{Yawing moment}}{qSb}$
C_Y	side-force coefficient, Side force/qS
C_μ	blowing coefficient, thrust produced by boundary layer control/qS
D	diameter, m (ft)
F_A	axial force, N (lbf)
F_N	normal force, N (lbf)
i_c	canard incidence, deg
ℓ	tail length m (ft)
q	free-stream dynamic pressure, N/m^2 (lbf/ft^2)
S	wing area, 10.232 m^2 (110.14 ft^2)
S_t	tail or canard area m^2 (ft^2)
T	engine thrust (thrust above the value for $T_c'=0$), N (lbf)

T_c'	thrust coefficient, T/qS
$T_c'=0$	thrust coefficient corresponding to the condition where the engine exhaust total pressure equals the free-stream total pressure
V	free-stream velocity, Kts (ft/sec)
X	longitudinal body axis
α	angle of attack, deg
β	angle of sideslip, deg
ε	downwash angle, deg
δ_f	trailing-edge flap deflection, deg
δ_j	static turning angle, deg
η	static turning efficiency

MODEL

The dimensional characteristics of the model are listed in Table I and shown in figure 2. A sketch of survey rake positions used in downwash measurements is shown in figure 3. Photographs of the model mounted for tests in the Langley full-scale tunnel are presented in figures 4 and 5. The model was constructed of wood and fiberglass over an aluminum frame and was essentially rigid for these low-speed tests.

The wing consisted of an arrow planform with an inboard leading-edge sweep angle of 74°, a mid-span sweep angle of 70.5°, and an outboard (27.5-percent of the semispan) sweep of 60°. It was mounted to the fuselage of the variable sweep model previously reported in reference 1. The wing (designed with twist and camber to provide good performance at a flight Mach number of 2.7) was constructed to stimulate the shape of an elastic wing in 1-g flight at low speeds. The thickness ratio was 3.08-percent, and the outboard 27.5-percent semispan leading edge was drooped 45°. The outboard trailing edge was drooped 5°. The wing had plain trailing-edge flaps that extended from the fuselage to the outboard vertical fins (see figs. 2(a) and 2(b)). A blowing slot, located forward of the leading edge of the left flap, was oriented to blow a sheet of high pressure air over the upper surface of the flap to control flow separation (fig. 2(c)). The trailing-edge flaps could be deflected from 0° to 30°.

The model was powered by two engine simulators mounted forward on the wing upper surface. The engine simulators consisted of tip-driven fans which were powered with externally supplied compressed air. The nozzle exits could be configured with 20° or 30° eyelid deflectors for turning the exhaust flow downward onto the wing upper surface.

Although most of the tests were conducted with the model in a tail-off configuration, the T-tail of reference 1 was installed for a limited number of tests.

TESTS AND CORRECTIONS

Force tests were conducted in the Langley full-scale tunnel for a range of Reynolds numbers (based on the wing mean aerodynamic chord) of 3.53×10^6 to 7.33×10^6. Tests were conducted for angles of attack from about -10° to 32°, and a few tests were conducted for side-slip angles of $\pm 5°$. Tests were conducted for flap angles of 0°, 10°, 20°, and 30°, with and without engines operating. The powered tests were made with and without deflectors attached to the engine exhaust nozzles. The value of thrust coefficient varied from 0 to 0.40; for a few tests, the left engine was inoperative while flap blowing (values of C_μ up to 0.10) was applied to the left flap to determine whether flap blowing could be used for controlling an engine-out situation.

Although the arrow-wing model was planned for tail-off tests only, the T-tail of reference 1 was installed for a limited number of tests in order to determine preliminary longitudinal stability and control characteristics of the model. The desired tail position for the arrow-wing configuration would probably be somewhat further aft than that of the T-tail as tested.

Downwash flow surveys were made at two chordwise planes in the vicinity of the T-tail. One plane was on the centerline of the horizontal tail pivot point ($\ell/\bar{c}$ = 0.982); the other survey was made further aft at $\ell/\bar{c}$ = 1.254. The survey covered a grid as indicated in figure 3 for four angles of attack. A calibrated pitch-yaw pitot static tube was used to measure the flow angles.

The test data have been corrected for air-flow angularity, bouyancy, and strut tares. Wall corrections were found by theory of reference 5 to be negligible and were not applied.

RESULTS AND DISCUSSION

Longitudinal Characteristics

Static Turning.- Since the effectiveness of a jet-flap system is dependent to a large extent upon the capability of the system to turn and spread the jet exhaust efficiently, static-turning tests were made of all the configurations included in the present investigation. The results are presented in figure 6 in terms of the ratio of normal force to thrust $F_{N/T}$ plotted against the ratio of axial force to thrust F_A/T. The results of figure 6 show, as expected, that very little turning occurred without the use of exhaust deflectors. The best turning performance was achieved with the 20° deflectors as indicated by efficiencies of 85 to 87 percent and turning angles closely approximating those of the geometric flap angle. The 30° deflectors gave poor static turning characteristics apparently because of excessive spreading which caused much of the jet exhaust to spread laterally off the flap.

Tail Off.- Presented in figure 7 are the results of tests to determine the effect of variations in Reynolds number from 3.53×10^6 to 7.33×10^6 on the

longitudinal characteristics of the wing-body combination. The data show that Reynolds number had only a small effect on the lift, drag, and pitching-moment characteristics of the model, particularly above a Reynolds number of 5.00×10^6. The majority of the tests were made at Reynolds numbers between 3.53×10^6 and 5.00×10^6.

Presented in figures 8(a) to 8(c) are the longitudinal characteristics of the wing-body combination for a range of thrust coefficients with the exhaust deflectors off. The data of figure 8(a) show that with the trailing-edge flaps undeflected the effect of thrust was to increase the lift-curve slope such that at an angle near the ground scrape angle (assumed to be 10° for this configuration) the lift coefficient was increased from about 0.4 to about 0.5 for $T_c' = 0.10$ and to C_L of about 0.55 for $T_c' = 0.20$. It is of interest to note that the increase in lift coefficient due to thrust is greater than that which could be accounted for by consideration of the direct component of the thrust vector ($T_c' \sin \alpha$), indicating that the engine exhaust above the wing apparently introduced favorable flow over the wing to increase lift. The pitching-moment data of figure 8(a) show the configuration to be neutrally stable at negative angles of attack and unstable at higher positive angles of attack with the level of instability increasing rapidly at angles of attack above about 15°. The abrupt increase in instability at the high angles of attack is similar to that shown for highly swept configuration of previous studies (for example, see ref. 6) and is associated with the vortex lift generated on the forward portion of the wing. This type of instability was eliminated in reference 6 by either deflecting the wing leading-edge or by increasing the wing leading-edge radius. No attempt was made to alter the wing leading-edge geometry in the present investigation because the primary

objective was to document the effects of USB on lift performance.

The data of figures 8(b) and 8(c) show similar effects of power for trailing-edge flap deflections of 10° and 20°. It should be noted, however, that with the deflectors off the lift increment produced by power was not as great at flap deflections of 10° and 20° as that produced at $\delta_f = 0°$ although the effect of increased flap deflection is to progressively increase the net lift coefficient.

The effect of installing exhaust deflectors on the model with trailing-edge flap deflections of 10° and 20° is shown in figures 9 and 10, respectively. A comparison of the data of figures 9 and 10 with those of figure 8 shows that, in general, the deflectors, as expected, increased the lift and generated large diving moments. The data of figures 9 and 10 show that the 20° and 30° exhaust deflectors gave about the same lift performance for a given geometric flap angle, but the 20° deflector did not penalize the thrust performance as much as the 30° deflector. This result is generally in agreement with the static-turning results of figure 6; although based on the static-turning data, the 30° deflector would be expected to produce much lower lift than that actually generated in the wind-on test. From these data, it was concluded that the 20° deflectors were probably more suitable from overall considerations, and the remainder of the program was conducted with the 20° deflectors.

The data of figure 11 show that substantially greater increments of lift were produced with 30° flap deflection than those for the 10° and 20° flap conditions. For example, at 10° angle of attack, a lift coefficient of about 0.9 was achieved with a thrust coefficient of 0.2 (fig. 11); whereas for the same thrust coefficient with 20° flap (fig. 10), a lift coefficient of about 0.8 was achieved. As expected, the higher flap setting produced larger diving

moments and resulted in more drag than that measured for the lower flap settings.

In order to better illustrate the effect of thrust in producing lift with the jet exhaust deflected downward over the trailing-edge flaps, the lift components which make up the total lift are presented in figure 12 for several trailing-edge flap deflections. The data of figure 12 show the values of circulation lift (C_{L_T}) as a function of T_c' for all flap deflections and, as expected, the 30° flap showed higher values of C_{L_T} than those produced by lower flap settings.

Downwash Characteristics.- Presented in figures 13 and 14 are the results of flow surveys to measure the downwash characteristics at several different vertical positions of the horizontal tail. The data show in general that the downwash angle was relatively small at the high tail positions. At the low tail position, the downwash angle was large and the variation of downwash angle with lateral displacement was very pronounced. The data of figures 13 and 14 are summarized in figure 15 in terms of the downwash factor $(1 - d\varepsilon/d\alpha)$ plotted against vertical tail height. The data of figure 15 show that the low tail positions gave values of $(1 - \partial\varepsilon/\partial\alpha)$ from about 0.1 to 0.2, indicating that a low horizontal tail position would be relatively uneffective from the standpoint of providing static longitudinal stability, and that a high tail position would probably be desireable.

Tail On.- In order to provide some preliminary information on longitudinal control effectiveness, tests were made using an existing horizontal tail from a previous investigation reported in reference 1. The vertical and horizontal-tail arrangement was used to obtain the control effectiveness data presented in figures 16(a) to 16(c). It should be noted that the data are not intended

to be representive of the tail effectiveness for a properly configured arrow-wing arrangement, but the data should serve as a guide in an analysis of the tail size and location required for the configuration. The data of figure 16(a) show that a -10° control incidence angle provided trim for the 30° flap condition with $T_c' = 0$; but for values of T_c' of 0.1 and 0.2, the diving moments could not be trimmed. Increasing thrust from $T_c' = 0$ to $T_c' = 0.20$ produced little change in the control effectiveness. The horizontal tail, which had an area of 5.8 percent of the wing area, provided a slight amount of longitudinal stability for the configuration in the low angle-of-attack range.

Pitch Trim Consideration.- One of the problems associated with the use of the USB concept is that the lift loads induced on the flaps produce large diving moments (see fig. 11). The magnitude of the problem of trimming the diving moments is illustrated in figure 16 by the fact that a modest sized conventional aft tail was inadequate for providing stability and trim for the powered-lift condition. Since the use of USB for high lift is dependent upon a satisfactory solution to the pitch trim problem, a brief study was made of the relative merits of several methods of providing pitch trim including:

1. A conventional aft tail
2. A free-floating canard
3. A fixed canard
4. A canard driven in proportion to α for artificial stability
5. A combination of canard and conventional tail

The effectiveness of the tails for providing trim and stability was examined for conditions corresponding to those obtained for the model with a trailing-edge flap deflection of 30° and a value of T_c' of 0.4 near $\alpha = 0°$. (See fig. 11). The analysis was conducted using the equations presented in reference 7 and

required the configuration to provide longitudinal trim, a three-percent static margin, and a trimmed lift coefficient of 0.7. For analysis purposes, the conventional tail and canard were assumed to have lift-curve slopes of 0.06 per deg, nondimensional tail lengths of 1.0, and downwash factors $\left(1 - \frac{\partial \varepsilon}{\partial \alpha}\right)$ of 0.5 and 1.0, respectively. For the geared canard, a lift-curve slope of -0.06 per deg was assumed, corresponding to a canard gear ratio $\frac{\Delta i_c}{\Delta \alpha} = -2.0$. A range of tail area ratios $S_{t/S}$ from 0 to 0.10 was evaluated; and the center of gravity position was allowed to vary so as to maintain a constant level of static margin as tail area increased. The results of the study are presented in figure 17 in terms of the tail lift coefficient $C_{L,t}$ required for the range of $\frac{S_t}{S}$.

The data of figure 17(a) show that the conventional tail tested in this investigation ($S_{t/S} = .058$) would require a lift coefficient of about 1.8 to provide trim and a three-percent static margin. A tail lift coefficient of 1.8 should be achievable with high-lift devices; however, additional control is required for normal flight operations, and a larger conventional tail would therefore be required. Increasing the size of a conventional tail has the advantage of shifting the neutral point of the configuration rearward to reduce the flap diving moment, but the conventional tail arrangement has the disadvantage of downward tail lift for trim which reduces the total lift of the airplane. In contrast to this condition, the fixed canard has the advantage of lifting upward for trim which increases the total lift, but it has the disadvantage of shifting the neutral point of the configuration forward. This forward shift in neutral point requires a forward shift in center of gravity (in order to maintain stability) which results in an increase in flap

diving moments. One means of achieving the lift benefit of the canard without its destabilizing effect is to have the canard free-floating (or have the canard mechanically driven such that its incidence angle does not change as the airplane angle of attack changes). Another approach would be to drive the canard surface such that its incidence angle is reduced as the airplane angle of attack is increased. This technique produces the benefits of both the canard and the conventional tail that is, an upward lift for trim and a rearward shift in the neutral point for reduced flap diving moments and increases stability. Figure 17(a) shows that such an arrangement can reduce appreciably the canard lift coefficient required for trim. In addition, it is possible to reduce the size of this type of canard arrangement when the canard is combined with a conventional horizontal tail. In this combination, the conventional tail would operate at zero lift or near zero lift in low-speed flight. In high-speed flight, the canard would be retracted and the conventional tail would be used for longitudinal control.

The results presented in figure 17(a) were determined on the basis that the configuration must maintain a static margin of three-percent for all conditions. Under this assumption, it was necessary to shift the center of gravity as the tail or canard size was changed, in order to keep the static margin constant. Figure 17(b) illustrates the center of gravity variation as a function of $S_{t/S}$ for each trim device investigated. The most significant point to be made regarding figure 17(b) is that the fixed or free-floating canard required a center-of-gravity location for low-speed flight forward of that required for supersonic cruise flight, creating a balance problem between the two speed ranges. In contrast, the conventional tail, the geared canard, or the combination geared-canard-plus-conventional tail permit the configura-

tion to be balanced at a center-of-gravity range consistent with that for supersonic cruise flight. In particular, the geared canard (alone or in combination with a more conventional tail) gives the desired low-speed center of gravity range with very small canard surfaces. From the results of figures 17(a) and 17(b), it is concluded that an all-movable, retractable canard in combination with a relatively small conventional tail would provide an efficient means of achieving stability and trim for a USB arrow-wing supersonic transport configuration in low-speed flight.

It is recognized that alternate approaches to the stability and trim problem are available, such as fuel management and relaxed static stability, and a comprehensive study beyond the scope of this paper is required to resolve the trade-offs and advantages of the various systems.

Performance Comparison.- In order to better show the relative performance of the model with exhaust deflectors off and on, the lift-drag polars for the model with several flap settings have been replotted in figure 18. For purposes of comparison, a 3° descent angle and a 3° climb angle are shown in each drag polar. On the assumption that the ratio of thrust coefficient to lift coefficient is equal to the ratio of thrust to weight (T/W), values of T/W for the 3° climb and descent conditions were determined from figure 18 and presented in figure 19 as plots of T/W against C_L. Also plotted in figure 19 is the ground scrape angle (10°) to help in establishing performance limits. It should be noted that for the data of figures 18 and 19 it was assumed that pitch trim could be achieved without penalizing the lift of the configuration. This assumption is based on the results of analysis presented in figure 17.

From the data of figure 19(a), it is seen that the maximum available lift coefficient for the model without deflectors is limited mostly by the

ground scrape angle and that the climb condition is much more critical than the glide condition in terms of the installed T/W ratio. The lift coefficient for the 3° climb condition is seen to increase from 0.50 up to about 0.73 by increasing the flap angle from 0° to 20° and by increasing the T/W ratio from 0.2 to 0.29. The 3° glide condition is seen to be limited to a lift coefficient of 0.70 for the 20° flap condition because of the ground scrape angle.

A comparison of the data of figure 19(a) and 19(b) shows that the use of exhaust deflectors increased the lift coefficient at which the 10° ground scrape angle occurred, but that higher values of T/W ratios are required to achieve the higher lift coefficients. It is readily apparent, therefore, that one critical factor in the use of the USB concept is the installed T/W ratio. For example, in figure 19(b), the 30° flap configuration would give a climb lift coefficient of about 1.1 at the ground scrape angle but would require a value of T/W of 0.40. Even for the 20° flap configuration, a value of T/W of about 0.35 would be required to achieve a C_L of 0.85 at the ground scrape angle. Since the maximum installed T/W ratio is likely to be no greater than about 0.3 for a four engine transport, it is seen that the climb lift coefficients produced by upper surface blowing would be limited to about 0.75 or 0.80 - values near those available with exhaust deflector off (fig. 19(a)).

For the approach condition, the data of figure 19(b) show an available lift coefficient of about 0.92 for the 30° flap configuration at the ground scrape angle and a value of T/W of only about 0.22. This condition suggests that higher flap angles could be utilized to increase the available approach lift coefficient without requiring excessively high values of T/W. From the data of figure 19, it therefore appears that an over-the-wing engine arrangement can be utilized most effectively in a supersonic transport configuration

by keeping the engine exhaust above the wing for take off and deflecting the exhaust onto the wing surface for landing.

Lateral-Directional Characteristics

Lateral-stability characteristics measured at sideslip angles of $\pm 5^\circ$ for the model with trailing edge flaps at 30° and for various thrust coefficients are presented for the tail-off and -on configurations in figures 20(a) and 20(b), respectively. Figure 20(a) shows that the model with tail-off was slightly directionally stable at negative angles of attack but became directionally unstable at the higher angles of attack. This result is very different from that found in previous investigation of arrow-wing configurations in which it was found that the directional stability for the tail-off condition increased with increasing angle of attack (for example, see ref. 6). This previous result was attributed to the fact that in a sideslipped condition the vortex flow from the leading wing produced a reversal of sidewash over most of the fuselage forward of the center of gravity. This sidewash produced a restoring yawing moment which made the configuration directionally stable. The fact that the present arrow-wing model with tail off was directionally unstable instead of stable probably results from flow interference between the wing and engines such that the wing vortex pattern was drastically altered. The data of figure 20(a) also show that the effective dihedral is positive ($-C_{l_\beta}$) and increased with increasing angle of attack to extremely large values near an angle of attack of 20°.

The data for the tail-on configuration (fig. 20(b)) show the model to be directionally stable up to an angle of attack of about 20°. Although the model became directionally unstable at higher angles of attack, increased thrust is seen to delay the angle of attack at which the instability occurred.

The effective dihedral for the tail-on configuration was generally similar to that for the tail-off configuration and in general the effects of thrust were relatively small.

Lateral Control Characteristics.- Presented in figure 21 are the lateral forces and moments produced by spoiler deflection. The spoiler was located aft of the left engine at a position directly forward of the inboard flap (see fig. 2). The data show that relatively large rolling and yawing moments were produced by spoiler deflection, indicating that the spoiler may be an effective lateral-control device in the propulsive-lift system for supersonic transport. The spoiler may also be useful for roll trim for the engine-out condition although the lift data of figure 21(b) show that the lift losses associated with 60° of spoiler deflection were very large.

Engine-Out Characteristics.- The problem of engine-out lateral trim can be very severe in a propulsive-lift system. To provide some fundamental information on the engine-out lateral problem of the present model, tests were conducted with the left engine inoperative and the results are presented in figure 22. Because in a powered-lift system a loss of an engine results in loss of lift, plots of the lateral characteristics with one engine inoperative are accompanied by plots of the corresponding longitudinal characteristics.

The data of figure 22(a) show that, as expected, large yawing and rolling moments were generated with an engine inoperative. The engine-out moments generally showed an increase with increasing angle of attack probably because the engine-out wing tended to stall first. Comparison of the corresponding lift data (fig. 22(b)) with lift data for symmetrical thrust (fig. 10) shows that large losses in lift also occur with engine failure.

Presented in figures 23 and 24 are the results of tests to study the use of asymmetric BLC over the flap of the engine-out wing as a means of providing roll trim. The data of figure 23 were obtained with blowing on the inboard flap segment only; whereas, the data of figure 24 were obtained with blowing over the two inboard flap segments. The data of figures 23 and 24 show that engine-out roll trim could be achieved up to moderate angles of attack with asymmetric blowing, but that excessively high values of C_μ were required. This result indicates that some other means of roll trim, such as spoiler deflection, differential flaps, or a combination of differential flaps with a small amount of asymmetric BLC would be more feasible than the use of BLC alone. Comparison of the lift data for asymmetric boundary layer control (fig. 24(b)) with that for symmetric thrust (fig. 10) shows that the use of BLC was effective for restoring the engine-out lift loss.

Presented in figures 25(a) and 25(b) are engine-out lateral-directional and longitudinal data, respectively, for the model with 30° trailing-edge flaps. Comparison of the data of figure 25 with those of figure 22 for the 20° flap condition shows that increasing flap deflection increased the engine-out rolling moment with the loss of an engine.

SUMMARY OF RESULTS

Force tests of a large-scale advanced arrow wing supersonic transport with engines mounted above the wing for upper surface blowing show the following results:

1. The USB concept was effective for providing the high lift required for improved take-off and landing performance.

2. Large diving moments accompanied the high propulsive lift. However, analysis indicates that a retractable, all-movable canard in combination with a relatively small conventional tail may be an effective arrangement for achieving longitudinal stability and trim at high lift.
3. The model exhibited static directional stability up to an angle of attack of about 20° and had high positive effective dihedral.
4. Spoiler deflection provided relatively large lateral control moments.
5. Large rolling and yawing moments were introduced with one engine inoperative. However, the use of asymmetric boundary layer control (BLC) on the trailing-edge flaps appeared to be one method of providing engine-out roll trim.

REFERENCES

1. McLemore, H. Clyde; Parlett, Lyle P.; and Sewall, William G.: Low-Speed Wind-Tunnel Tests of A 1/9-Scale Model of A Variable-Sweep Advanced Supersonic Transport. NASA TM X-71960, 1974.

2. McLemore, H. Clyde; and Parlett, Lyle P.: Low-Speed Wind-Tunnel Tests of A 1/10-Scale Model of a Blended-Arrow Advanced Supersonic Transport. NASA TM X-72671, 1975.

3. Morris, Odell A.; and Fournier, Roger H.: Aerodynamic Characteristics At Mach Numbers 2.30, 2.60 and 2.96 Of A Supersonic Transport Model Having A Fixed, Warped Wing. NASA TM X-1115, 1965.

4. Morris, Odell A.; and Patterson, James C., Jr.: Transonic Aerodynamic Characteristics of A Supersonic Transport Model With A Fixed, Warped Wing Having 74° Sweep. NASA TM X-1167, 1965.

5. Heyson, Harry H.: Use of Superposition In Digital Computers To Obtain Wind-Tunnel Interference Factors For Arbitrary Configuration, With Particular Reference To V/STOL Models. NASA TR R-302, 1969.

6. Freeman, Delma C., Jr.: Low Subsonic Flight and Force Investigation Of A Supersonic Transport Model With A Highly Swept Arrow Wing. NASA TN D-3887, 1967.

7. Johnson, Joseph L.: Wind-Tunnel Investigation Of The Static Longitudinal Stability and Trim Characteristics Of A Sweptback-Wing Jet-Transport Model Equipped With An External-Flow Jet-Augmented Flap NACA TN 4177, 1958.

Table 1

DIMENSIONAL CHARACTERISTICS OF MODEL

Wing:	
Area, m^2 (ft^2)	10.232 (110.14)
Span, m (ft)	4.191 (13.750)
Aspect Ratio	1.72
Spanwise Station of Mean Aerodynamic Chord, m (ft)	0.642 (2.105)
Incidence Relative to Horizontal Reference Line, deg	-5.240
Root Chord, m (ft)	4.608 (18.399)
Mean Aerodynamic Chord, m (ft)	3.368 (11.050)
Tip Chord, m (ft)	0.540 (1.772)
L. E. Sweep (STA 49.87 STA 187.31), deg	74.00
L. E. Sweep (STA 187.31 STA 247.38), deg	70.50
L. E. Sweep (STA 247.38 STA 286.64), deg	60.00
Vertical Tail:	
Area, m^2 (ft^2)	0.823 (8.859)
Span, m (ft)	0.760 (2.493)
Sweep Angle:	
L. E., deg	37.00
T. E., deg	30.00
Root Chord m (ft)	1.900 (6.234)
Tip Chord m (ft)	0.640 (2.100)
Vertical Fin (Two):	
Area, m^2 (ft^2) (Total)	0.415
Span, m (ft)	0.328 (1.075)

Aspect Ratio (each)	0.517
Sweep Angle:	
L. E., deg	73.40
T. E., deg	16.40
Root Chord, m (ft)	1.109 (3.638)
Tip Chord, m (ft)	0.158 (0.518)
Horizontal Tail:	
Area, m^2 (ft^2)	0.651 (7.197)
Span, m (ft)	1.420 (4.667)
Length of Mean Aerodynamic Chord, m (ft)	0.500 (1.640)
Incidence, deg	-20-+5
L. E. Sweep Angle, deg	45.00
Root Chord, m (ft)	0.700 (2.297)
Tip Chord, m (ft)	0.240 (0.792)

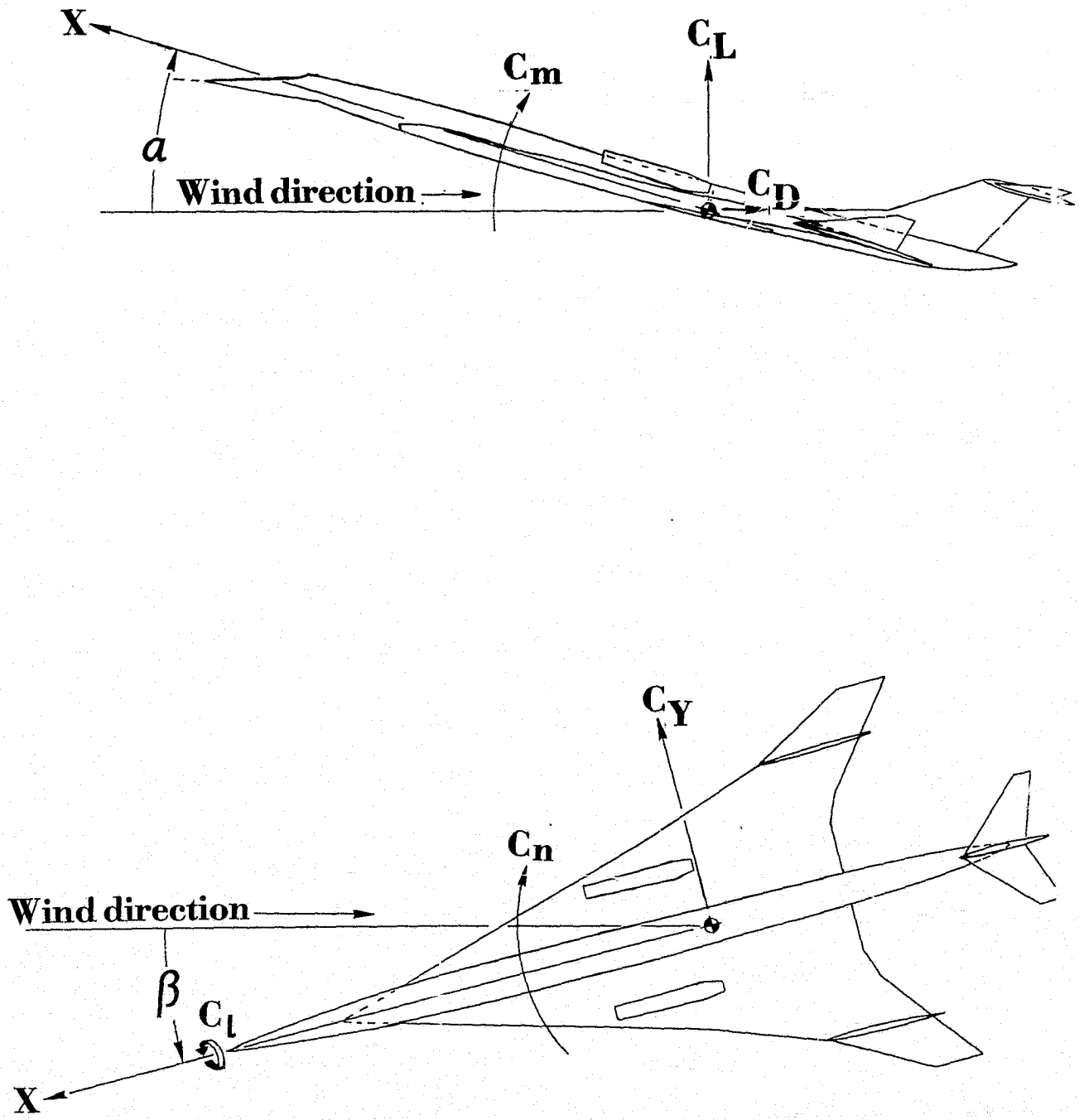

Figure 1.- The body system of axes.

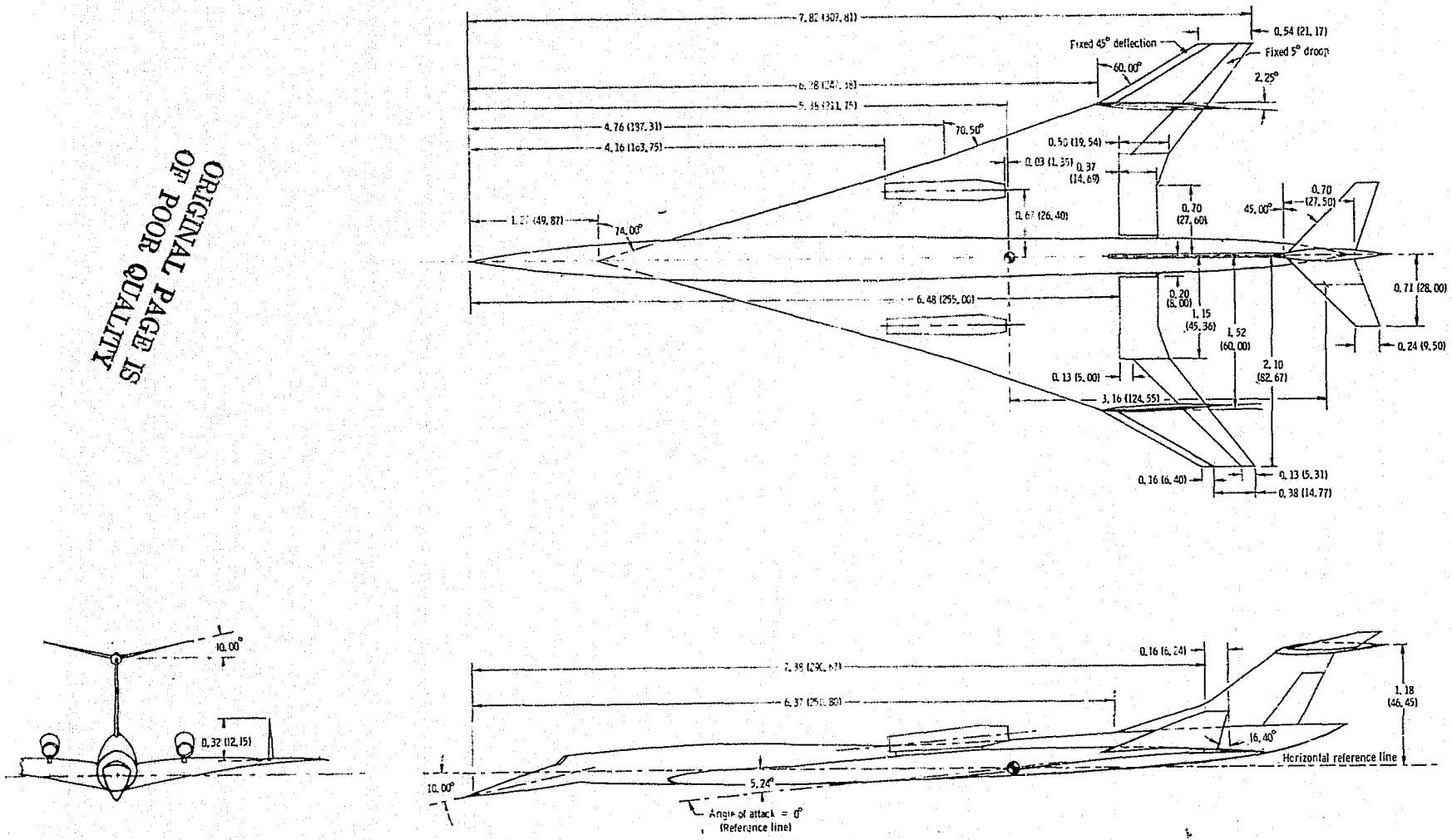

(a) Three-view drawing of model.

Figure 2.- Dimensional characteristics of model. Dimensions in meters (inches).

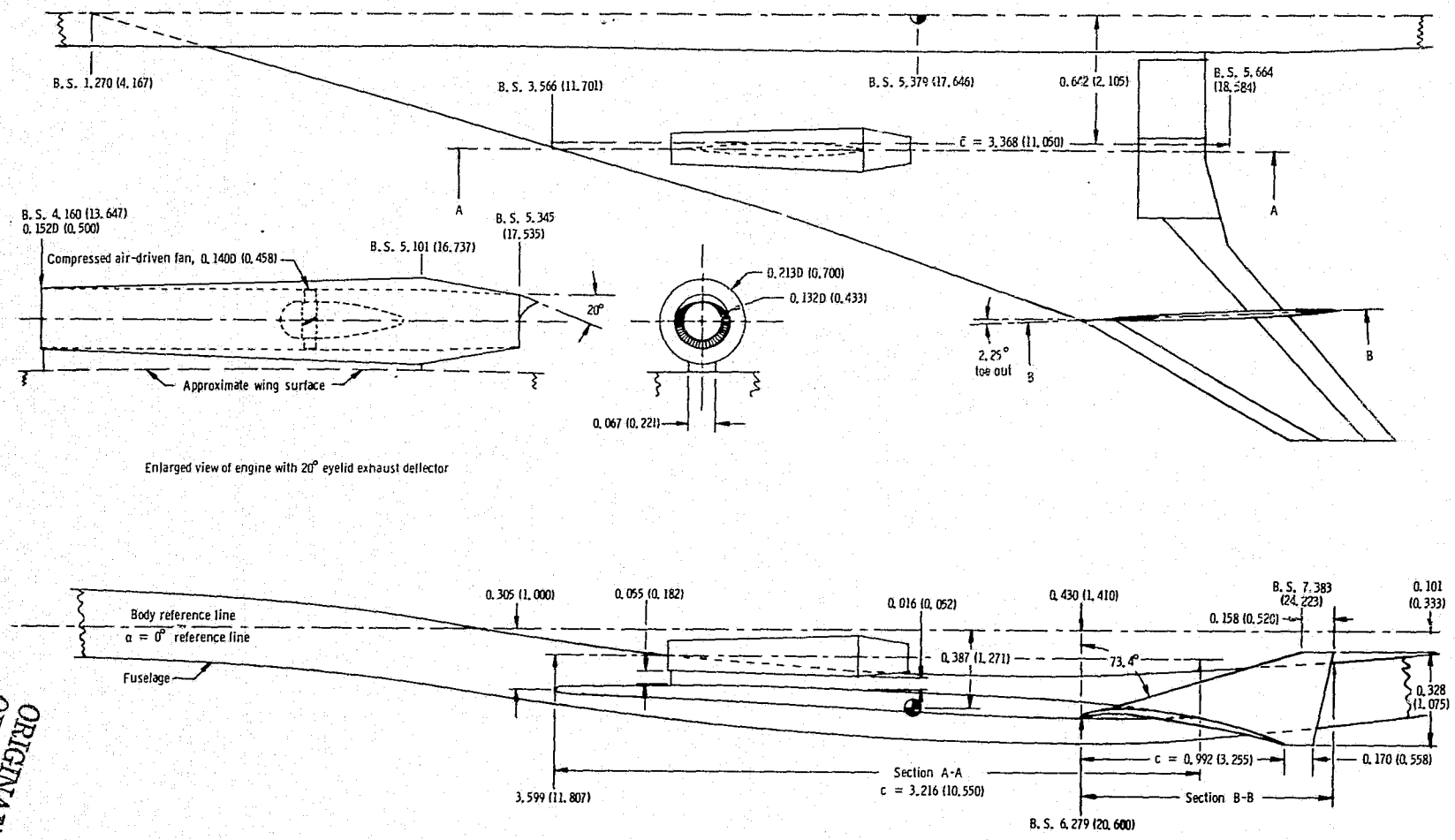

(b) Geometric relationships at engine and fin stations. All dimensions in meters (feet).

Figure 2.- Continued.

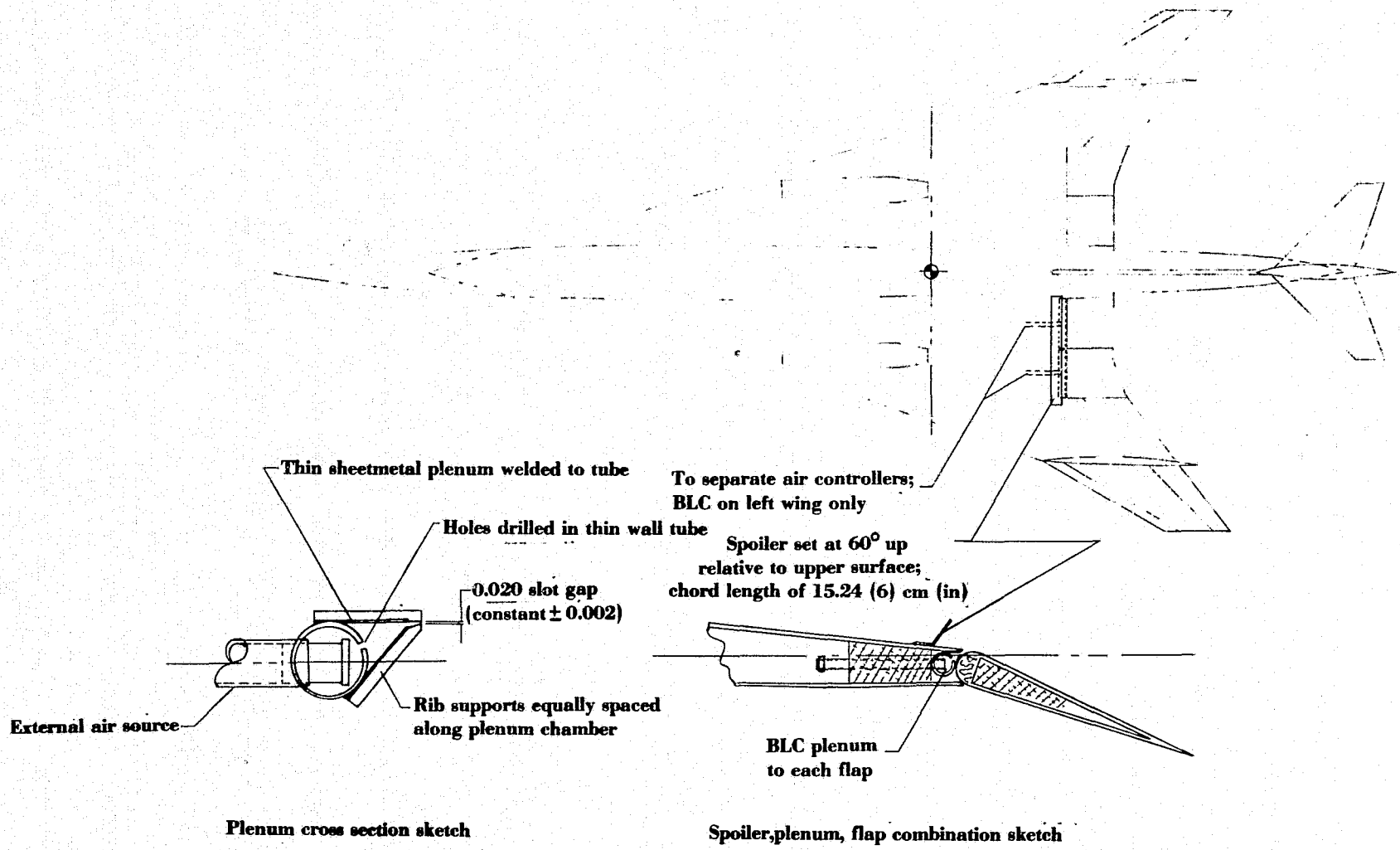

(c) Sketch of flap boundary layer control and spoiler installation.

Figure 2.- Concluded.

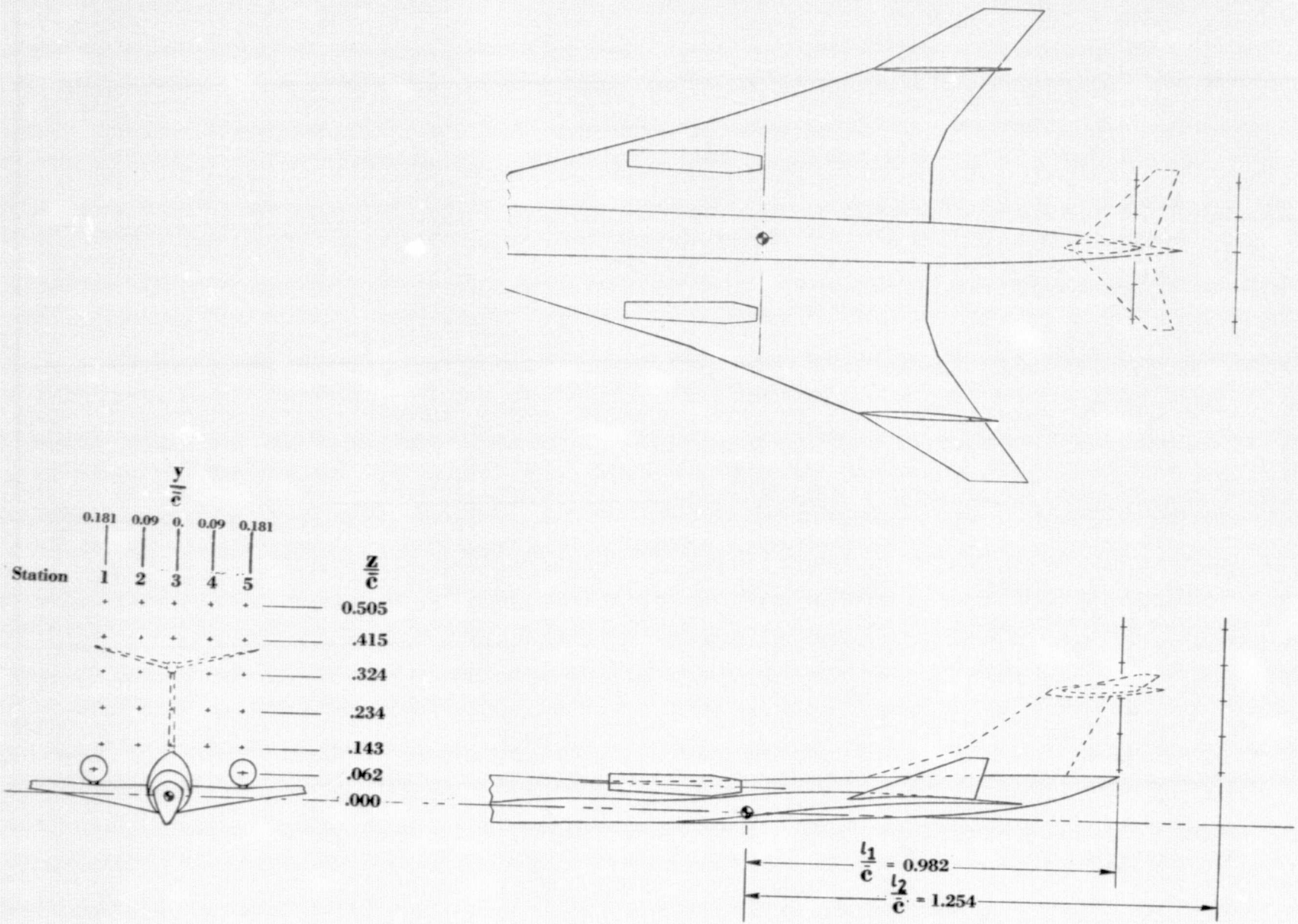

Figure 3.- Location of downwash survey rake positions for the tail off configuration.

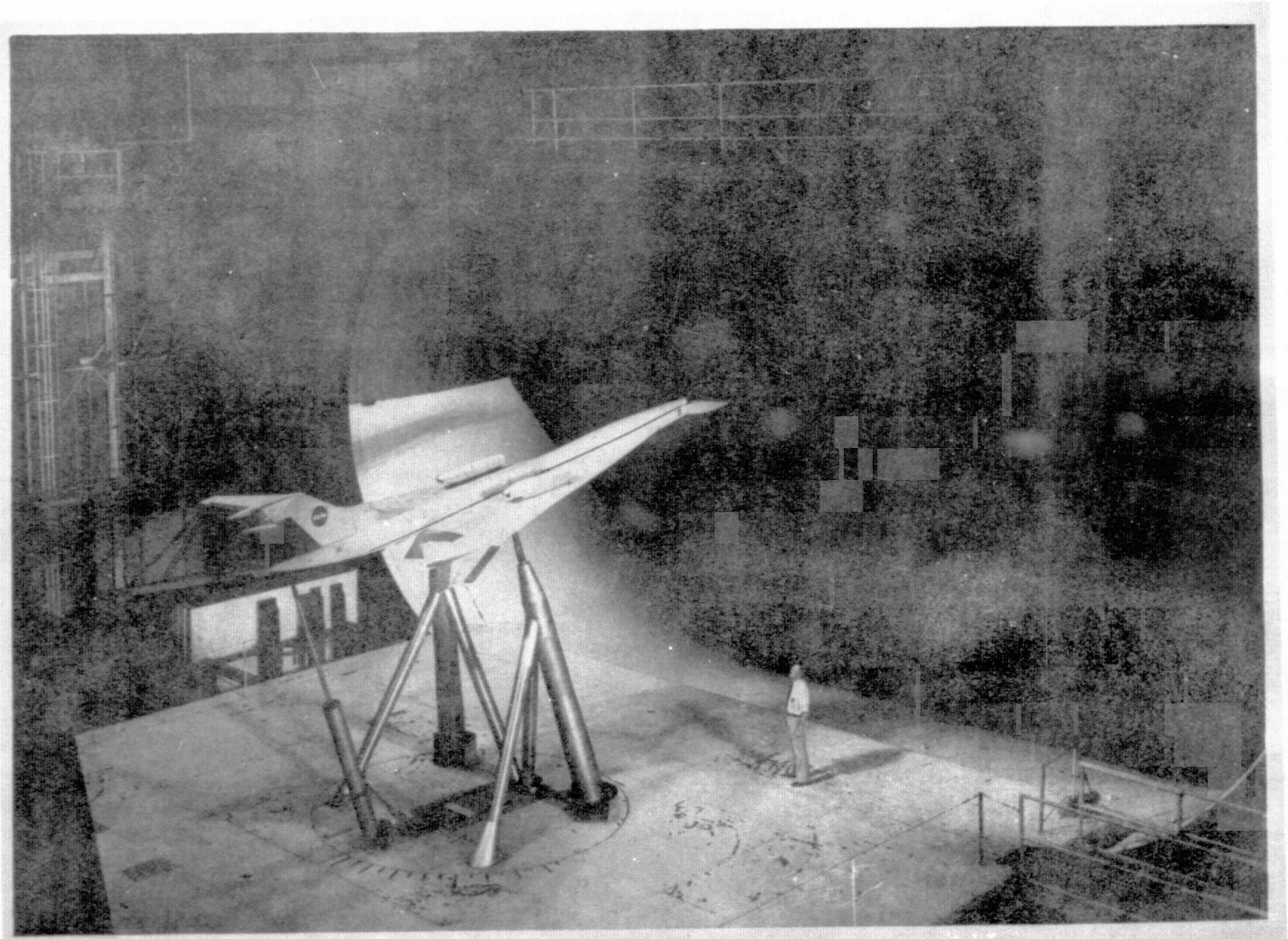

Figure 4. - Three - quarter rear view of the model mounted for tests in the Langley full - scale tunnel.

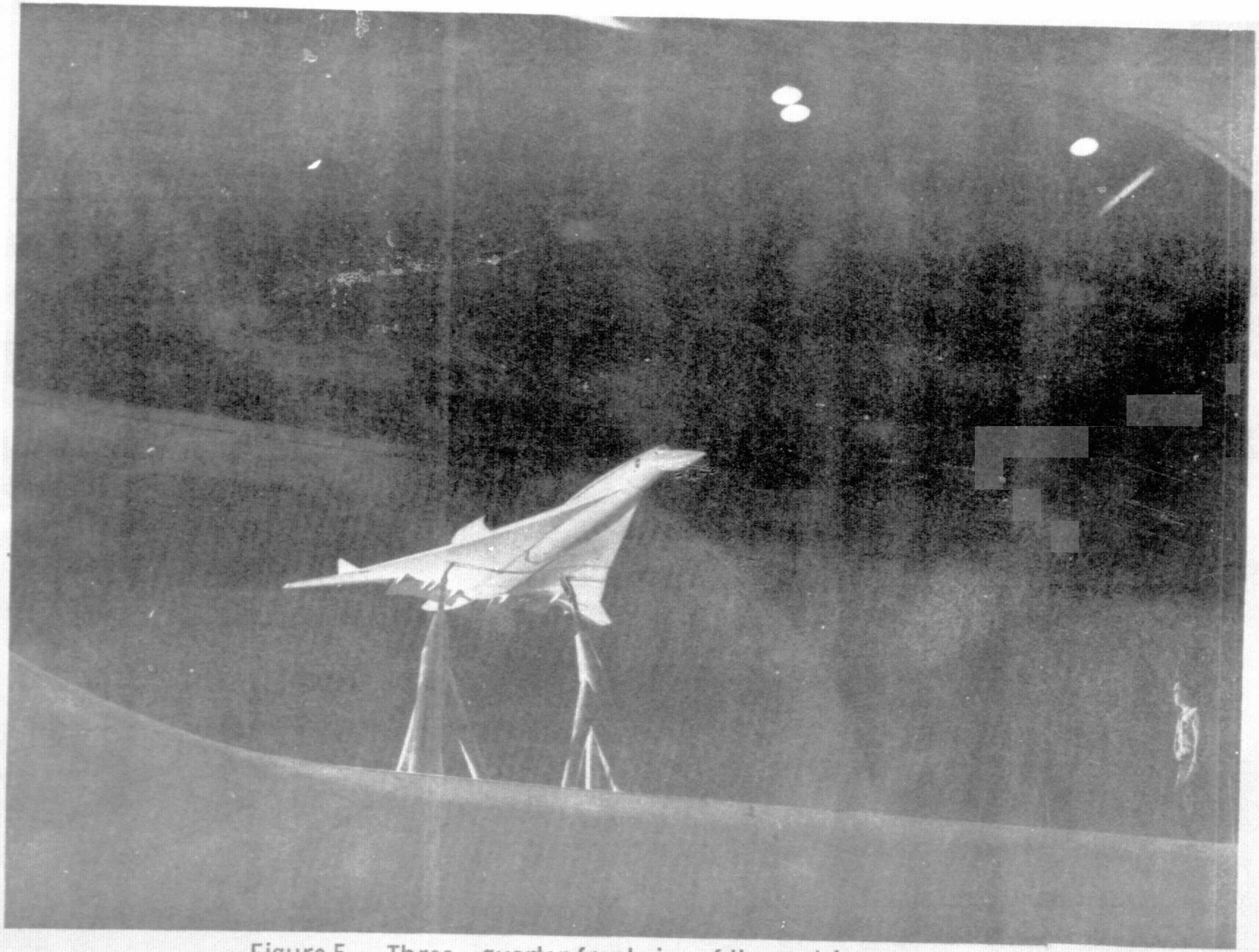

Figure 5. - Three - quarter front view of the model mounted for tests in the Langley full - scale tunnel.

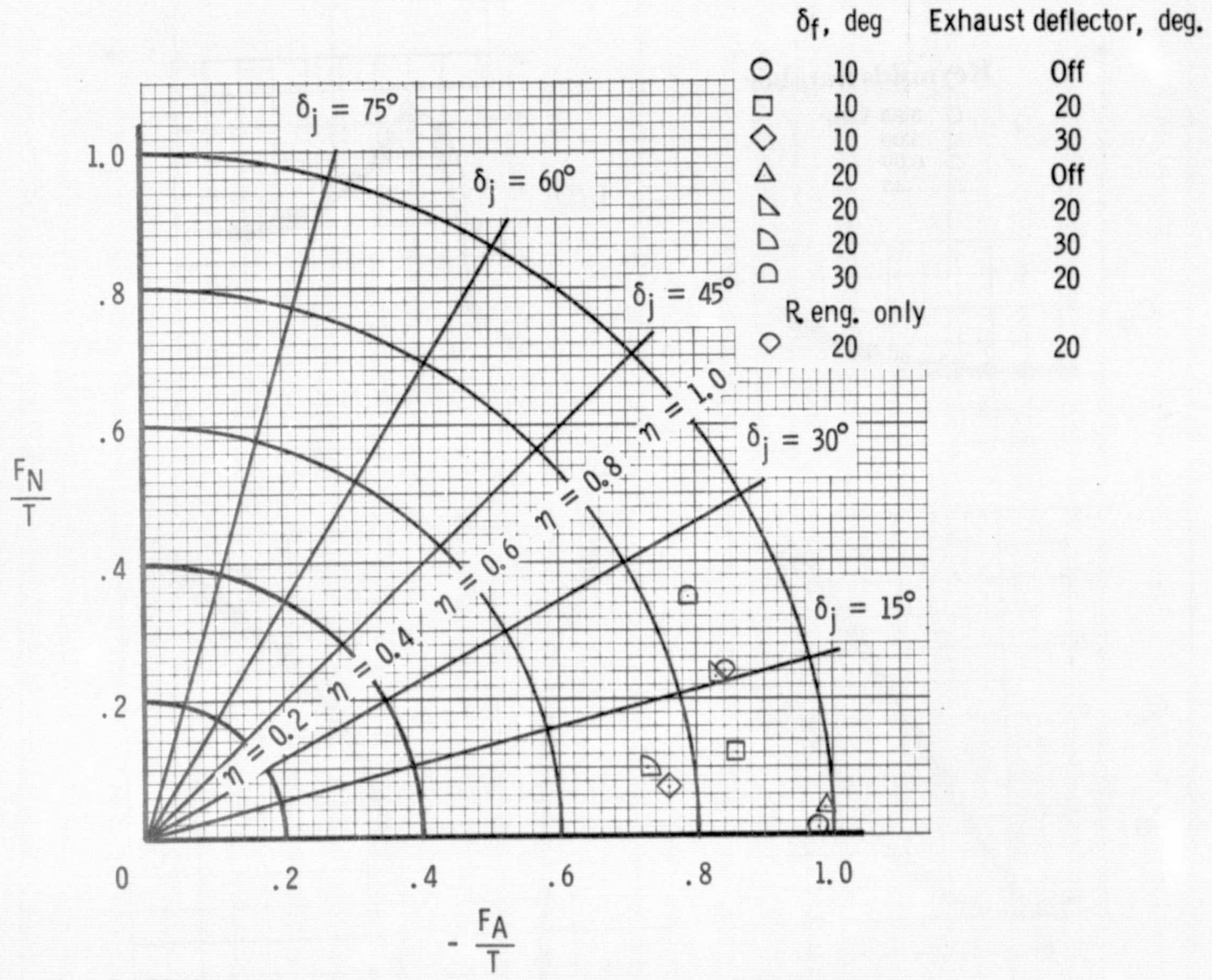

Figure 6 . - Static turning performance.

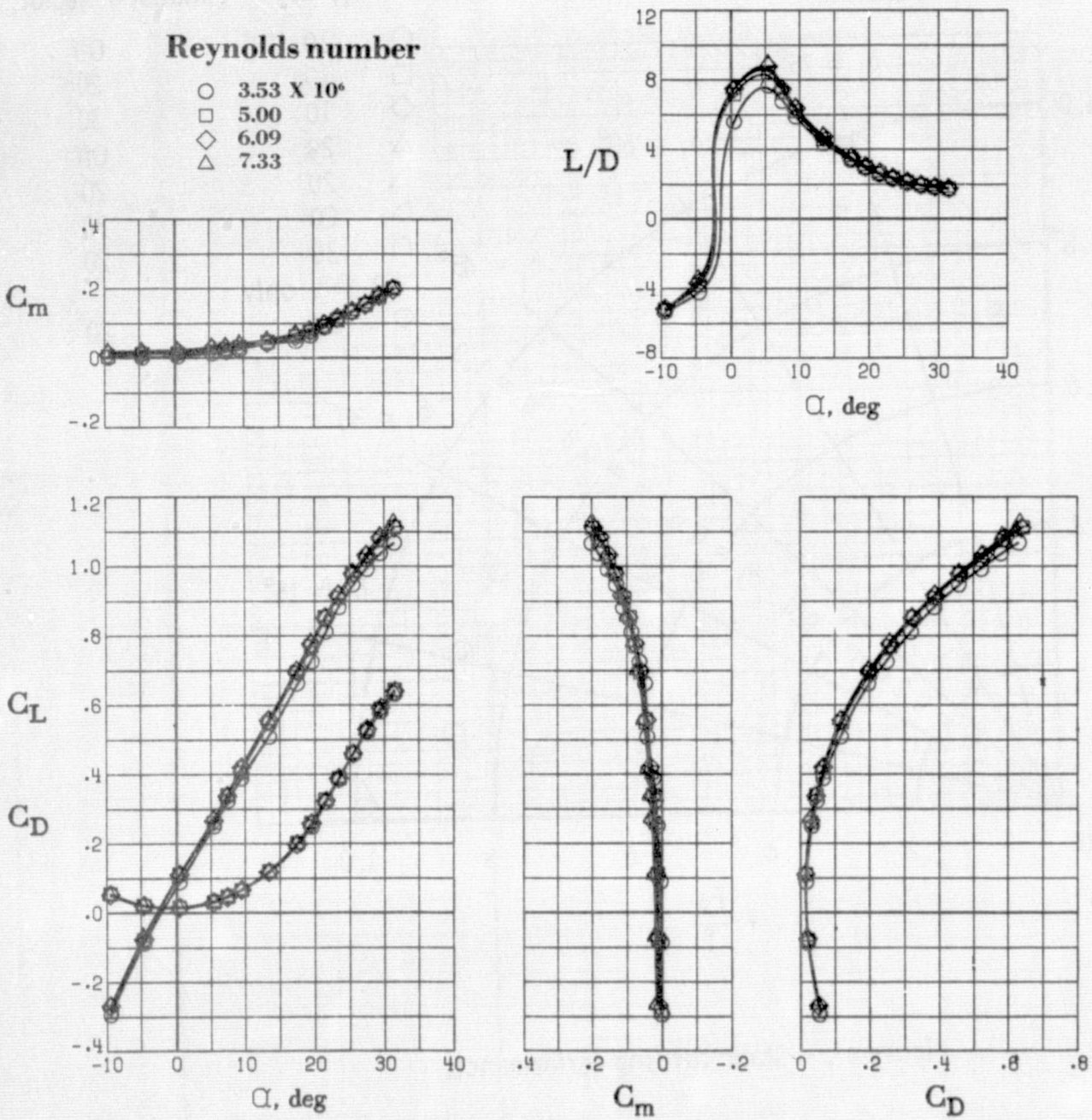

Figure 7.- Effect of Reynolds number on longitudinal aerodynamic characteristics. $\delta_f = 0°$. $T_c' = 0$.

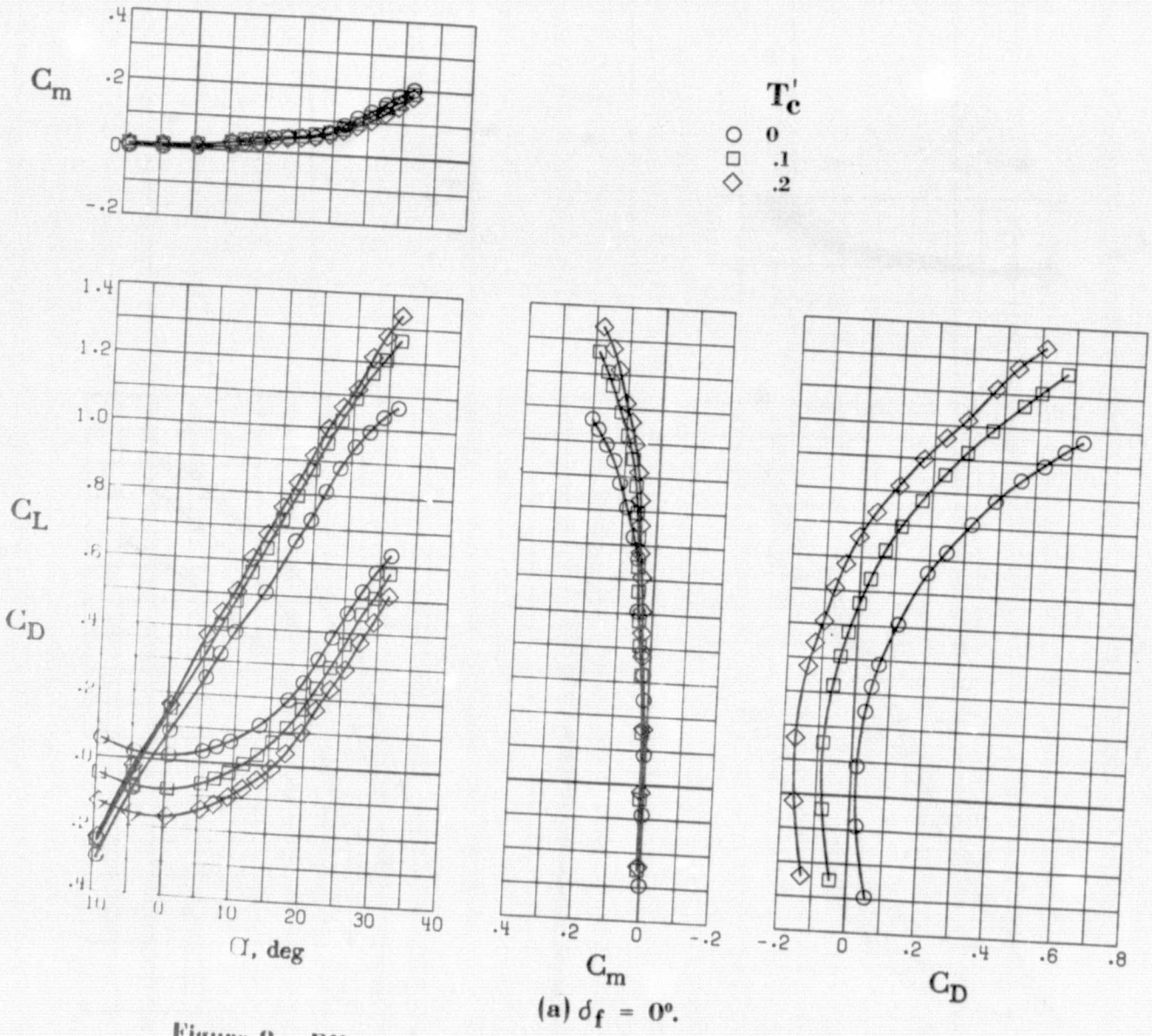

(a) $\delta_f = 0°$.

Figure 8.- Effect of thrust on longitudinal aerodynamic characteristics. No exhaust deflectors on engines.

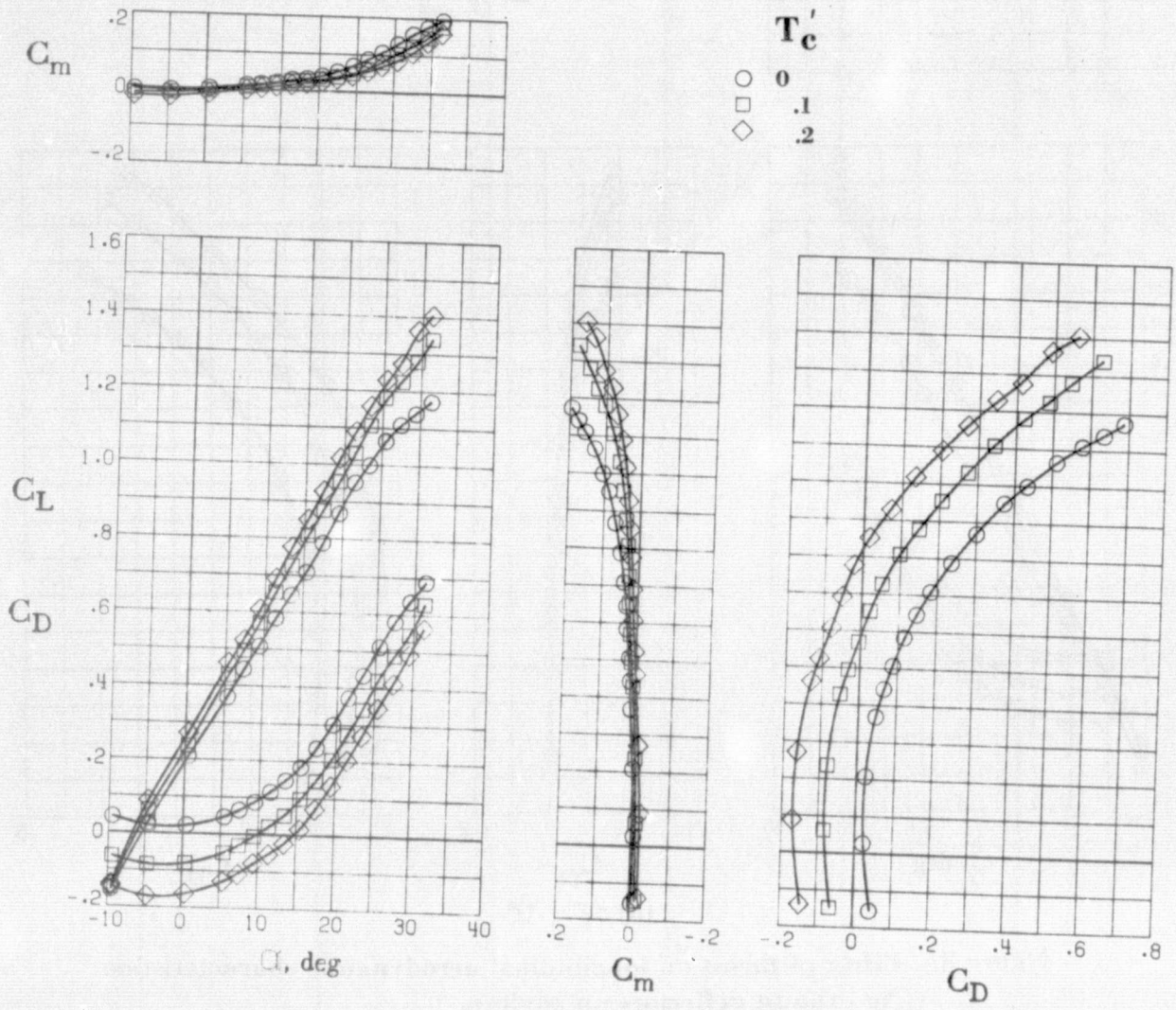

(b) $\delta_f = 10°$.

Figure 8.- Continued.

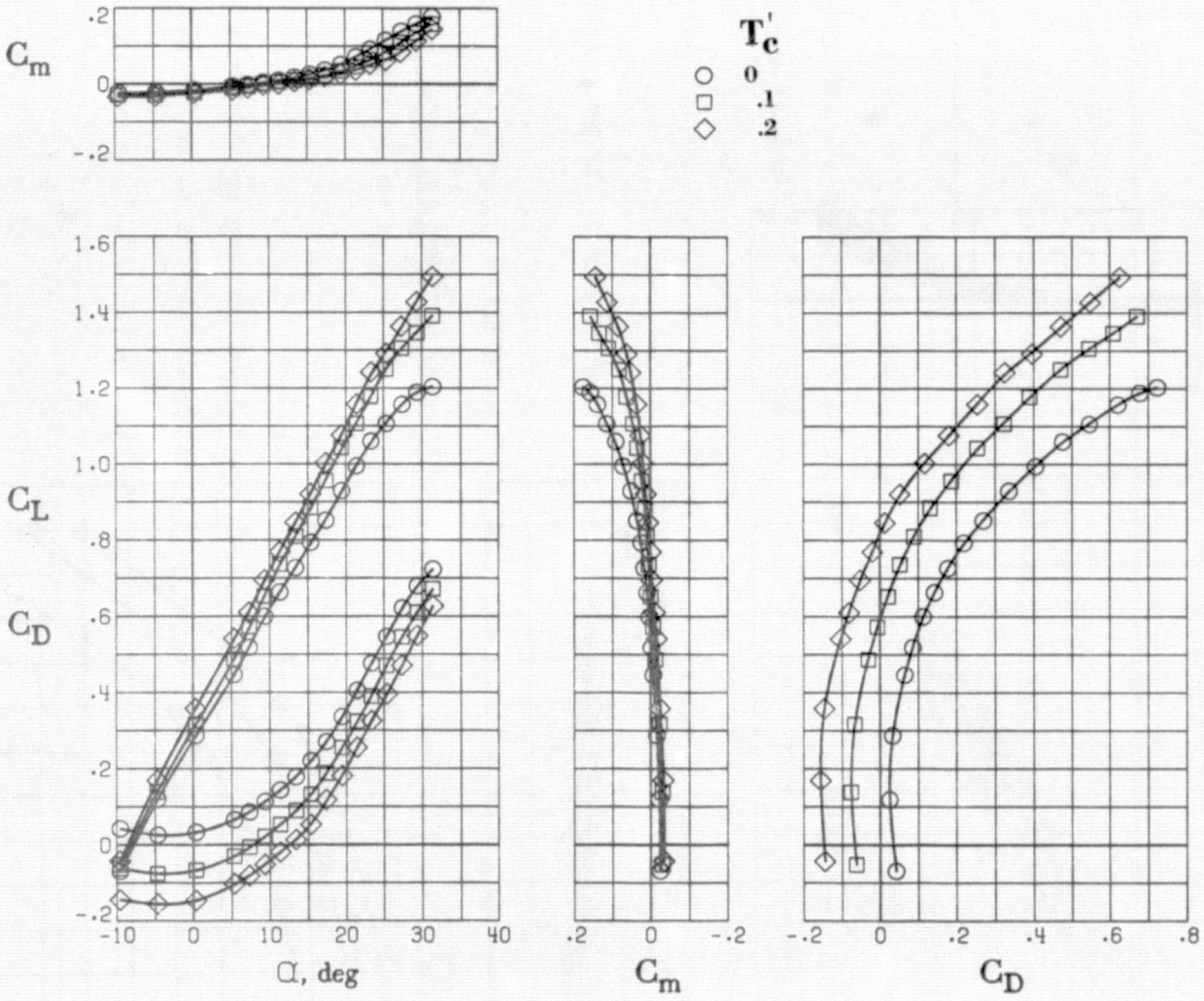

(c) $\delta_f = 20°$.

Figure 8.- Concluded.

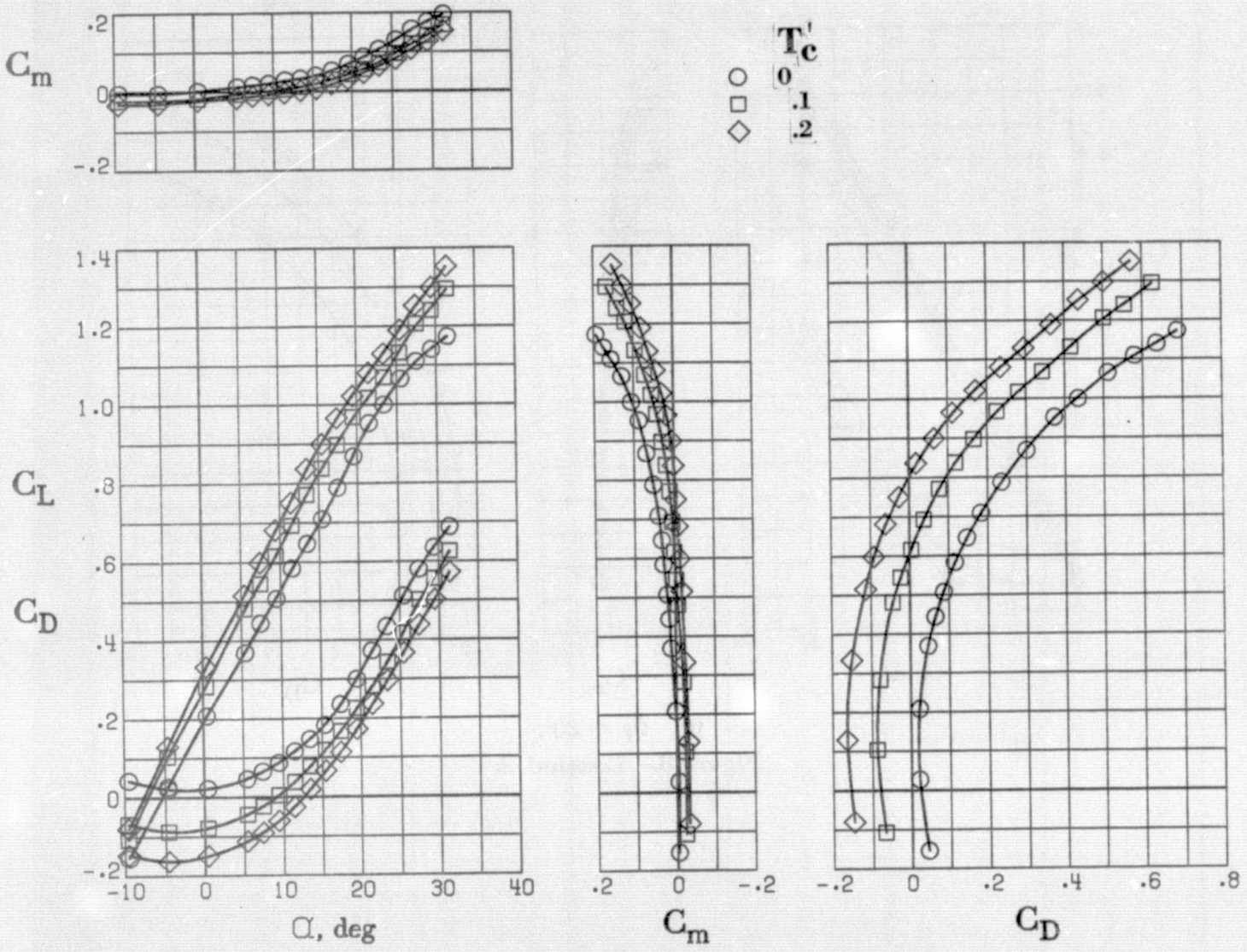

(a) 20° Exhaust deflectors installed.

Figure 9.- Effect of thrust on longitudinal aerodynamic characteristics. $\delta_f = 10°$.

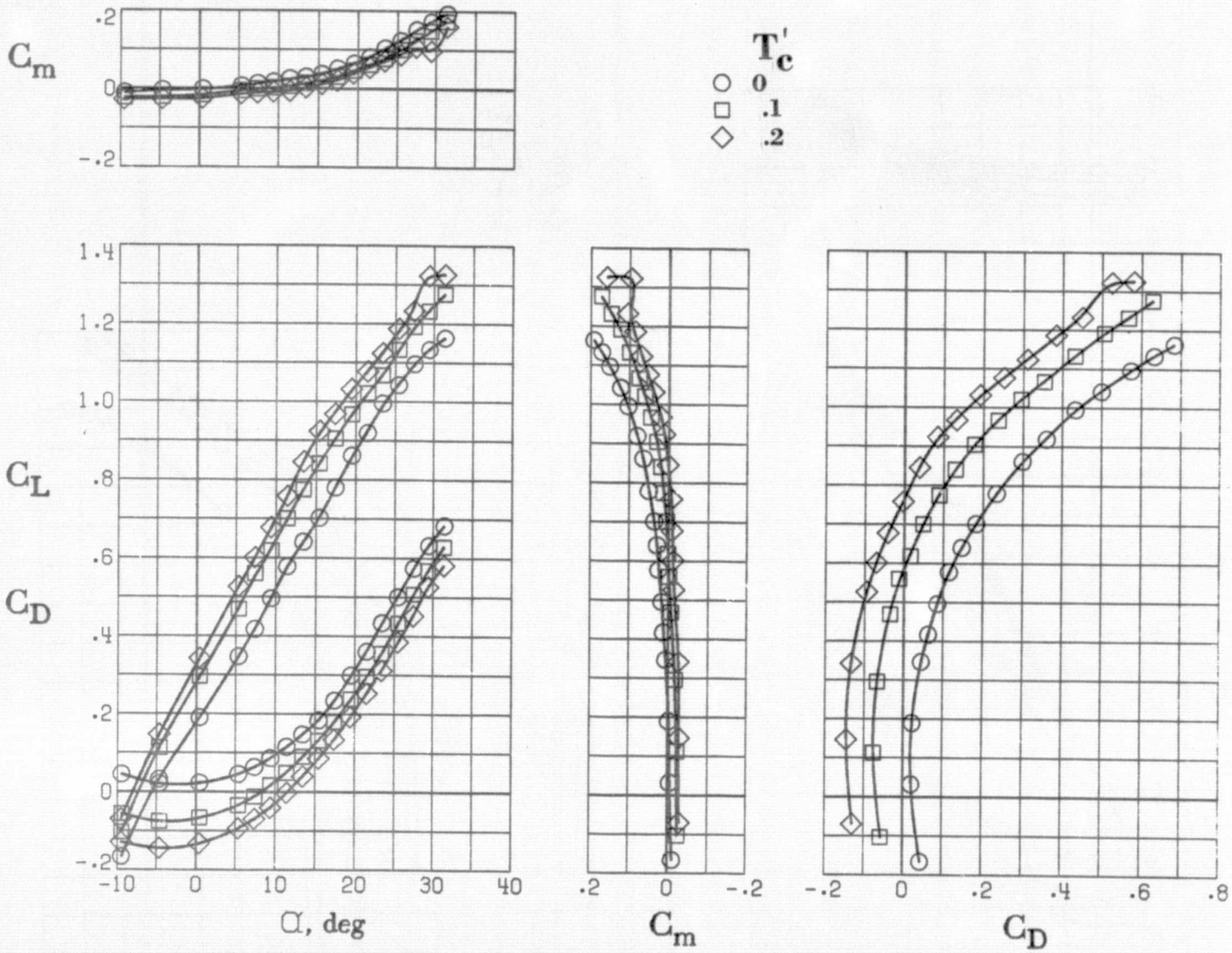

(b) 30° Exhaust deflectors installed.

Figure 9.- Concluded.

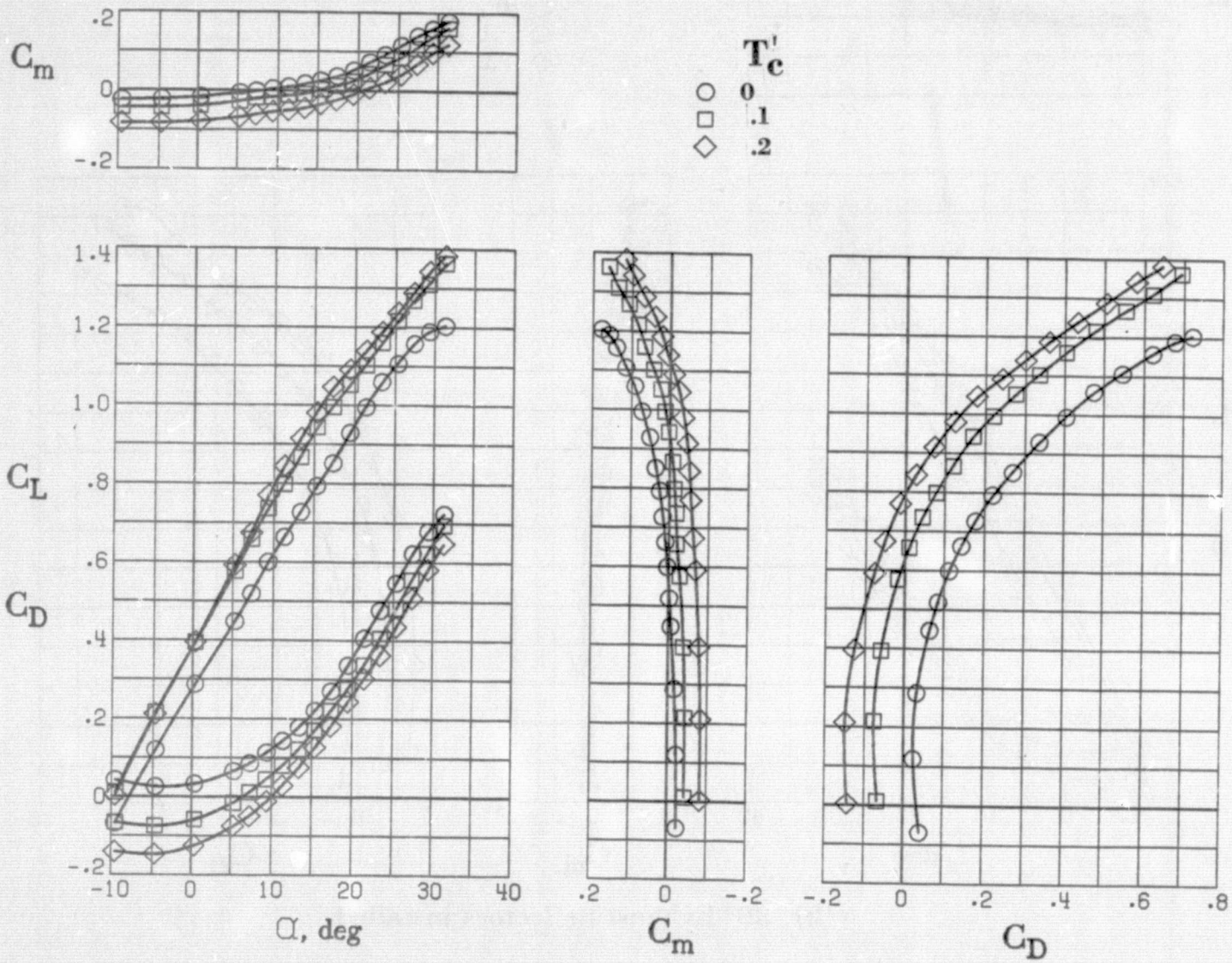

(a) 20° Exhaust deflectors installed.

Figure 10.- Effect of thrust on longitudinal aerodynamic characteristics. $\delta_f = 20°$.

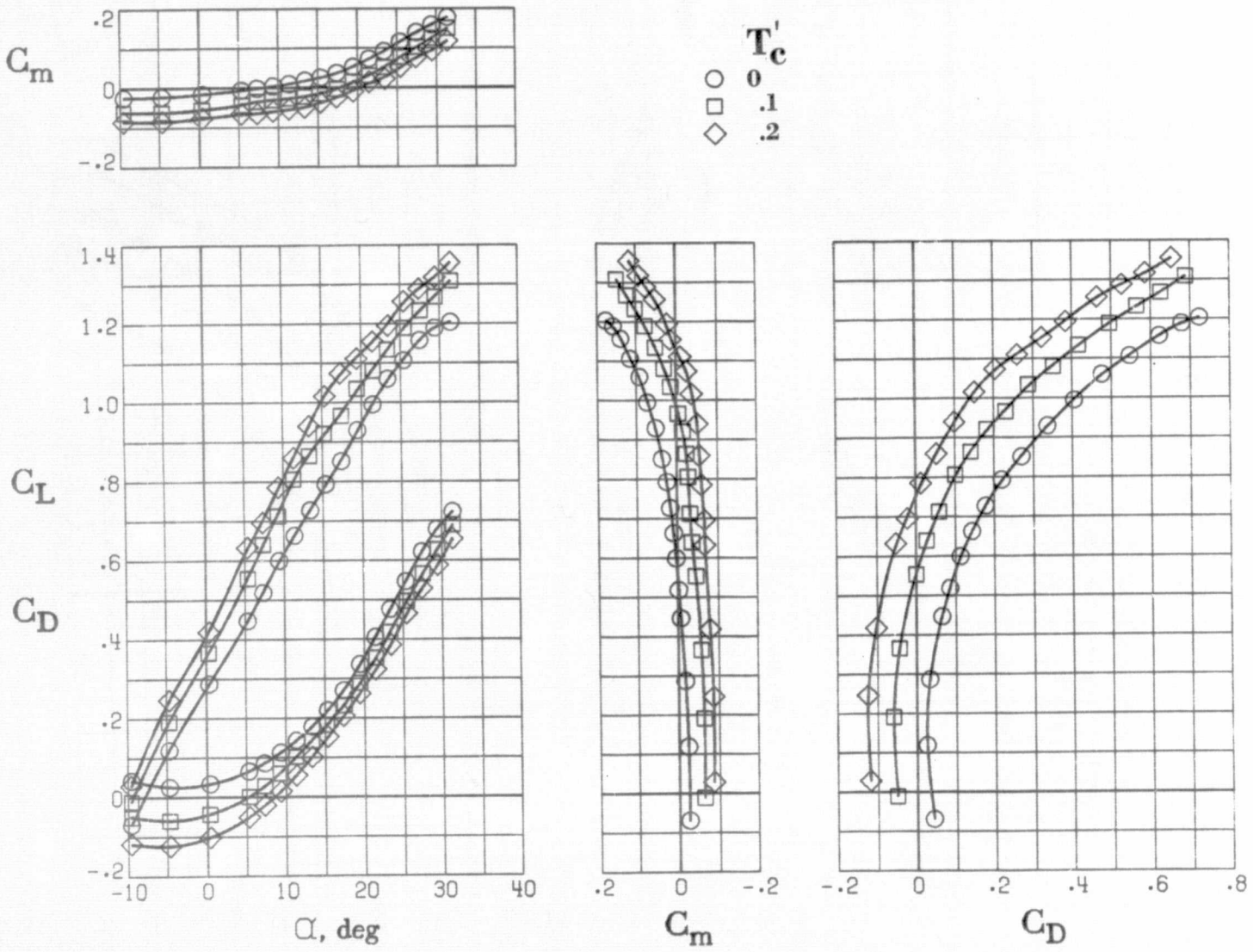

(b) 30° Exhaust deflectors installed.

Figure 10.- Concluded.

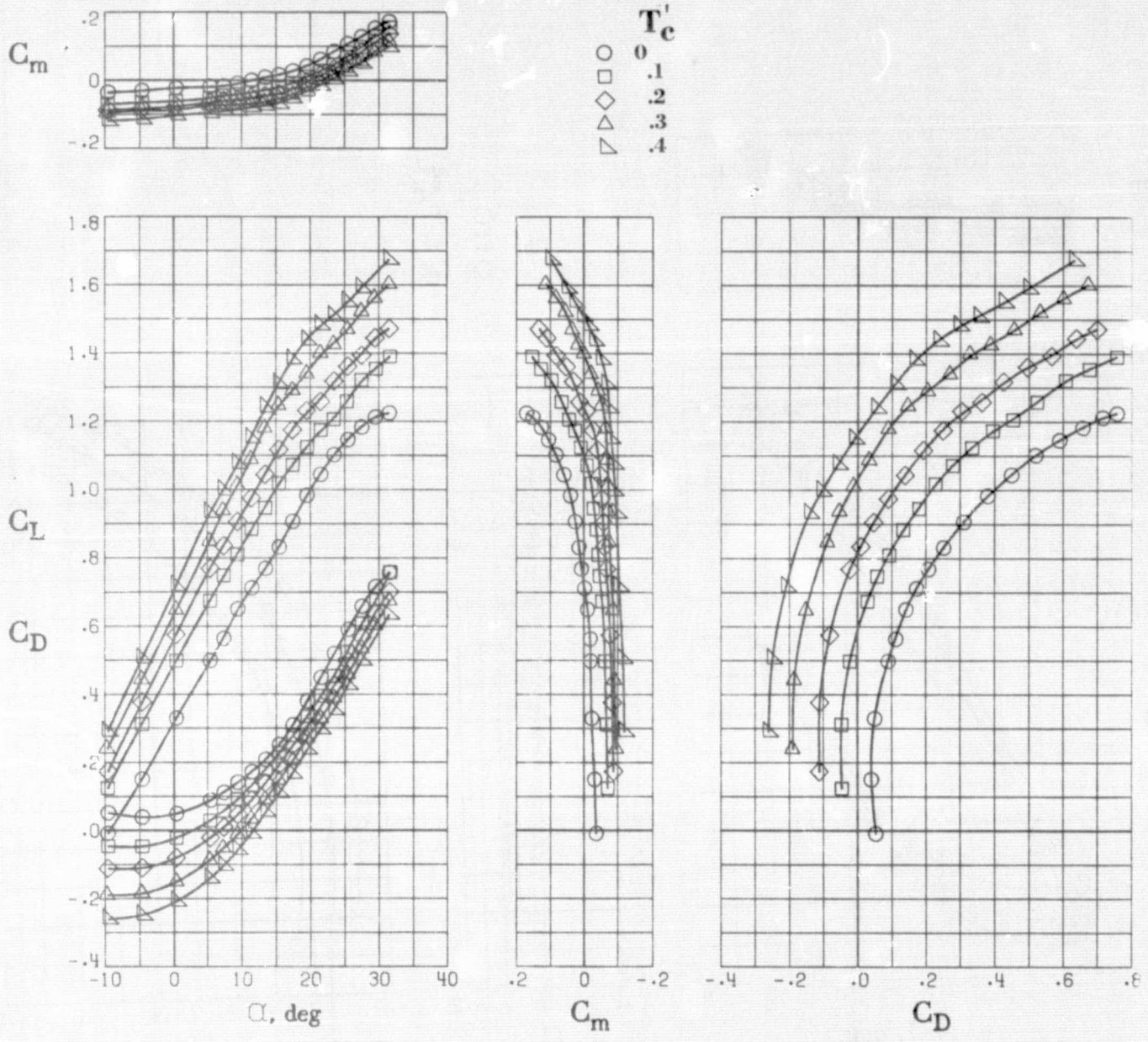

Figure 11.- Effect of thrust on longitudinal aerodynamic characteristics. $\delta_f = 30^o$. 20^o Exhaust deflectors installed.

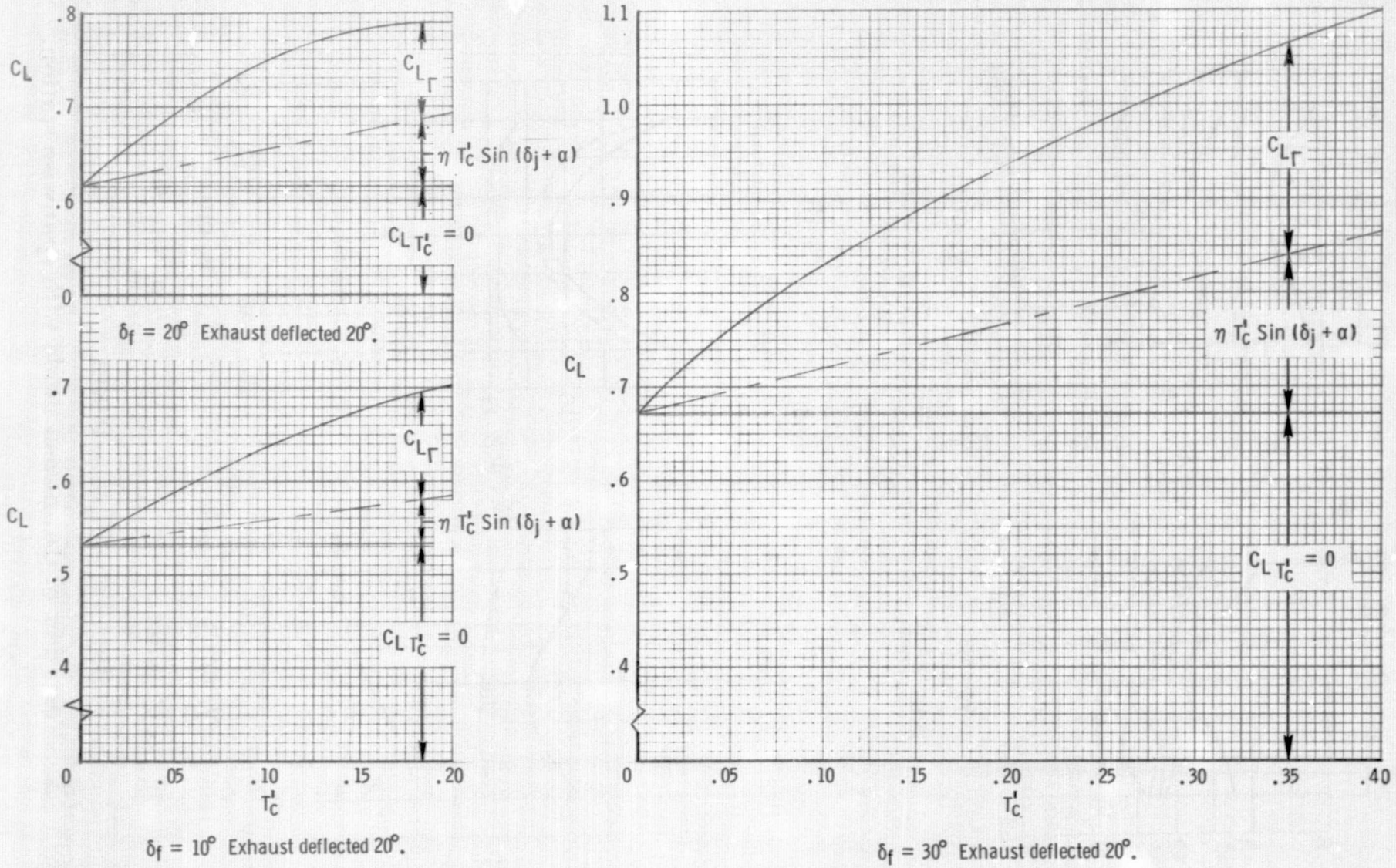

Figure 12.- Variation of lift components with thrust coefficient.

$\alpha = 10°$.

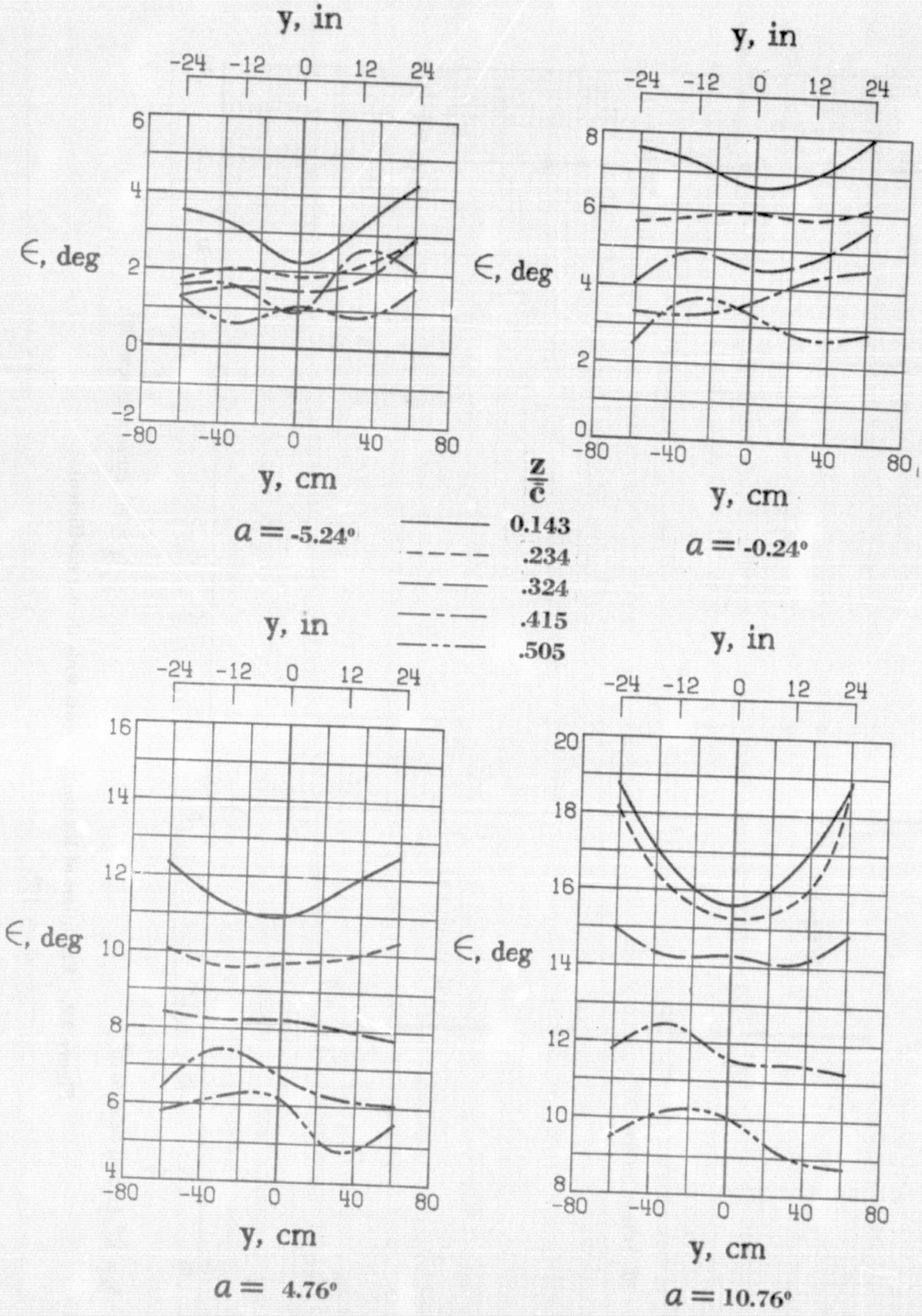

(a) $Tc' = 0$; $t/\bar{c} = 0.982$.

Figure 13.- Variation of downwash angle with spanwise station. $\delta_f = 20°$. Deflectors off.

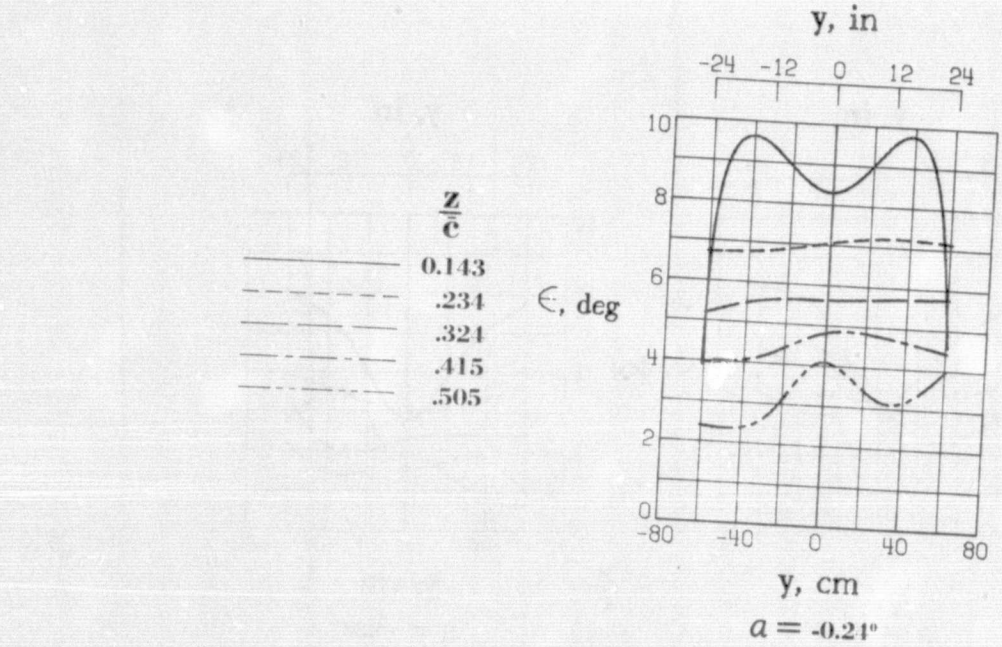

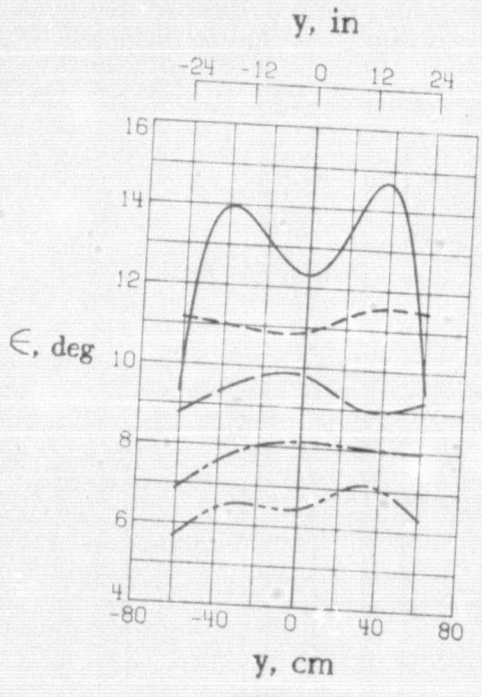

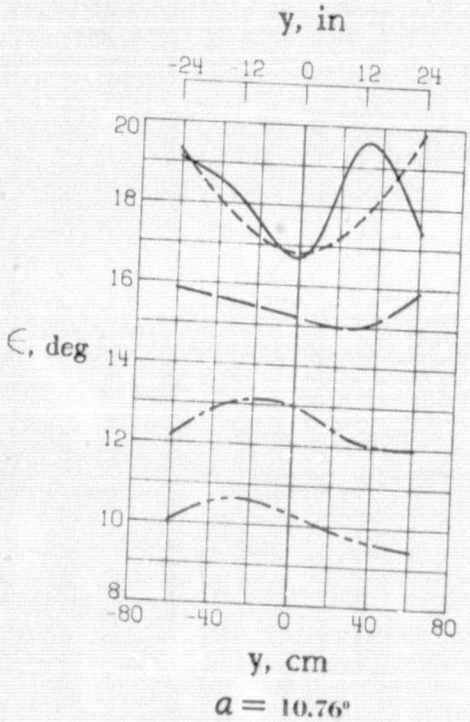

(b) $Tc' = 0.2$; $t/\bar{c} = 0.982$.

Figure 13.- Continued.

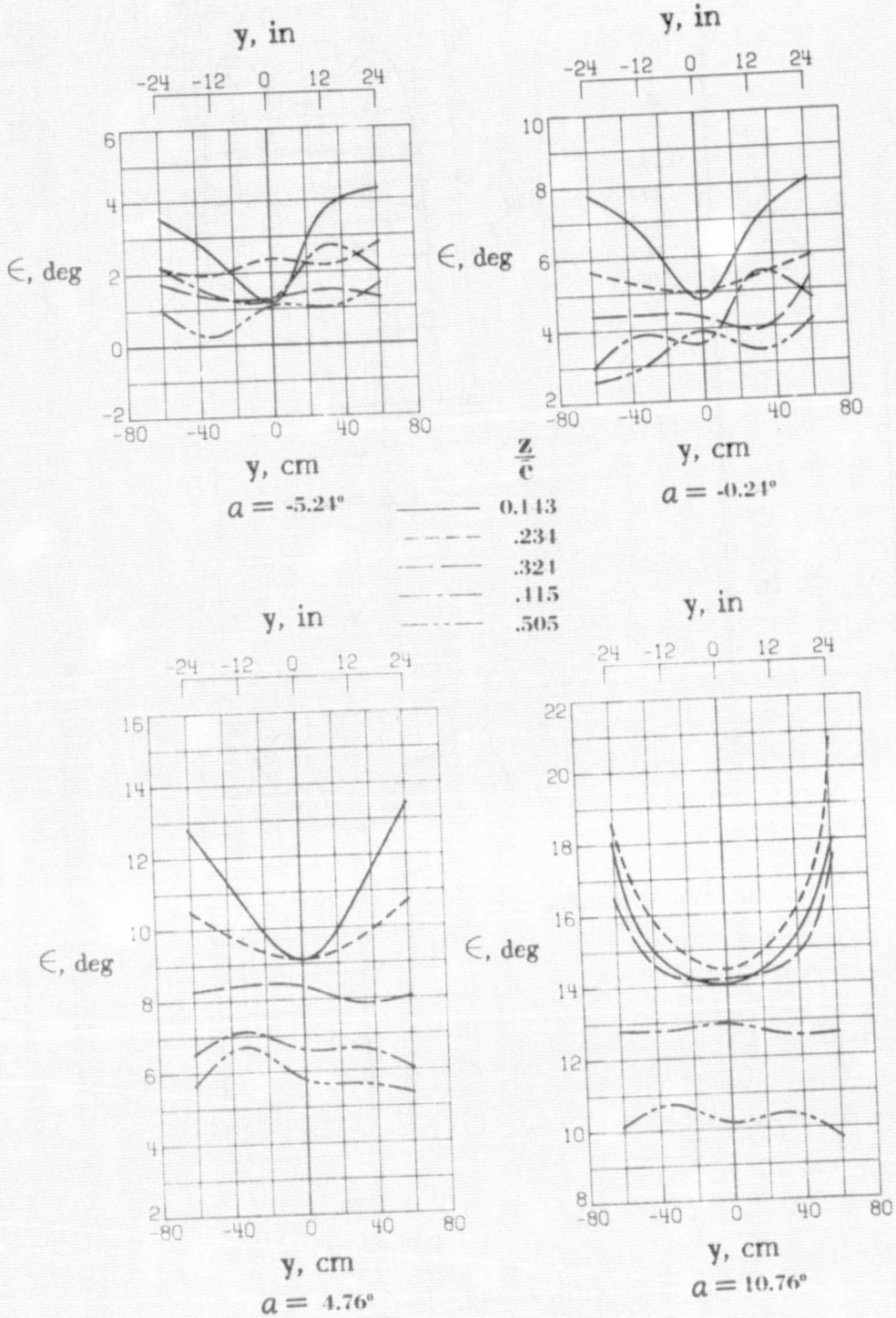

(c) $T_c' = 0$; $t/\bar{c} = 1.254$.

Figure 13.- Continued.

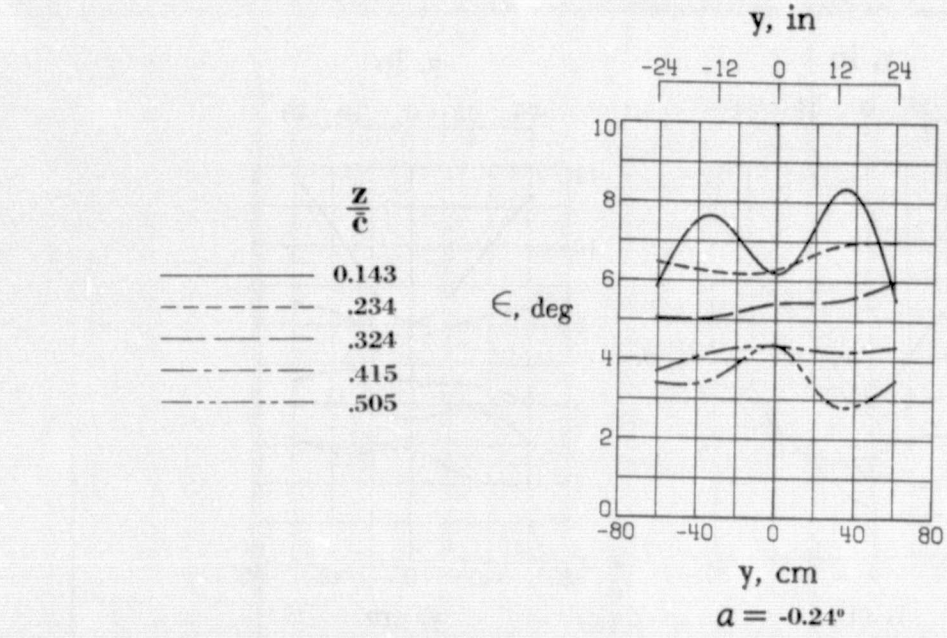

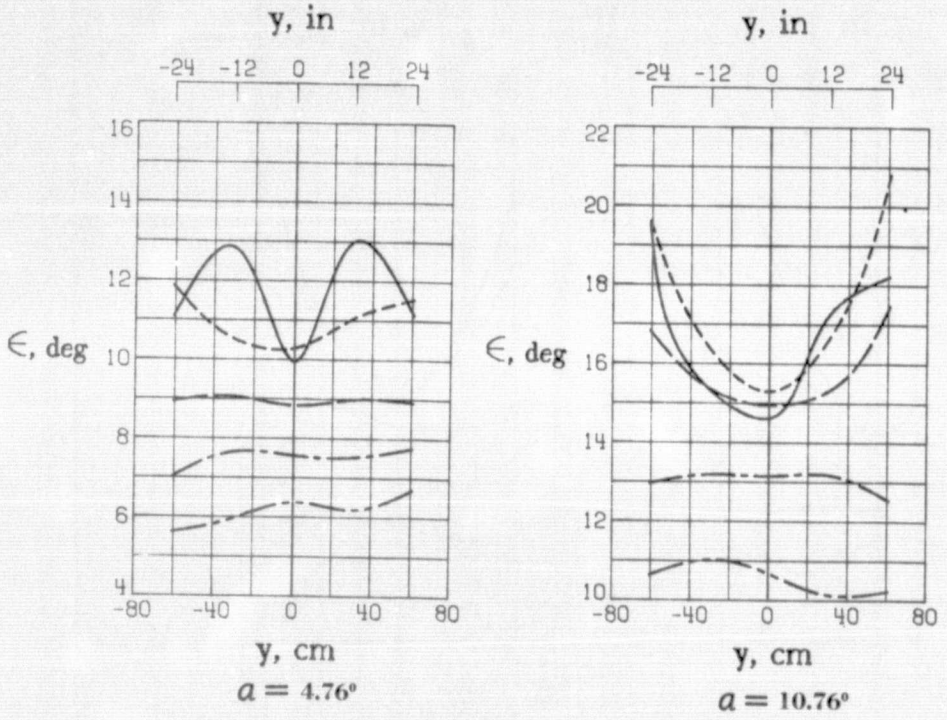

(d) $Tc' = 0.2$; $t/\bar{c} = 1.254$.

Figure 13.- Concluded.

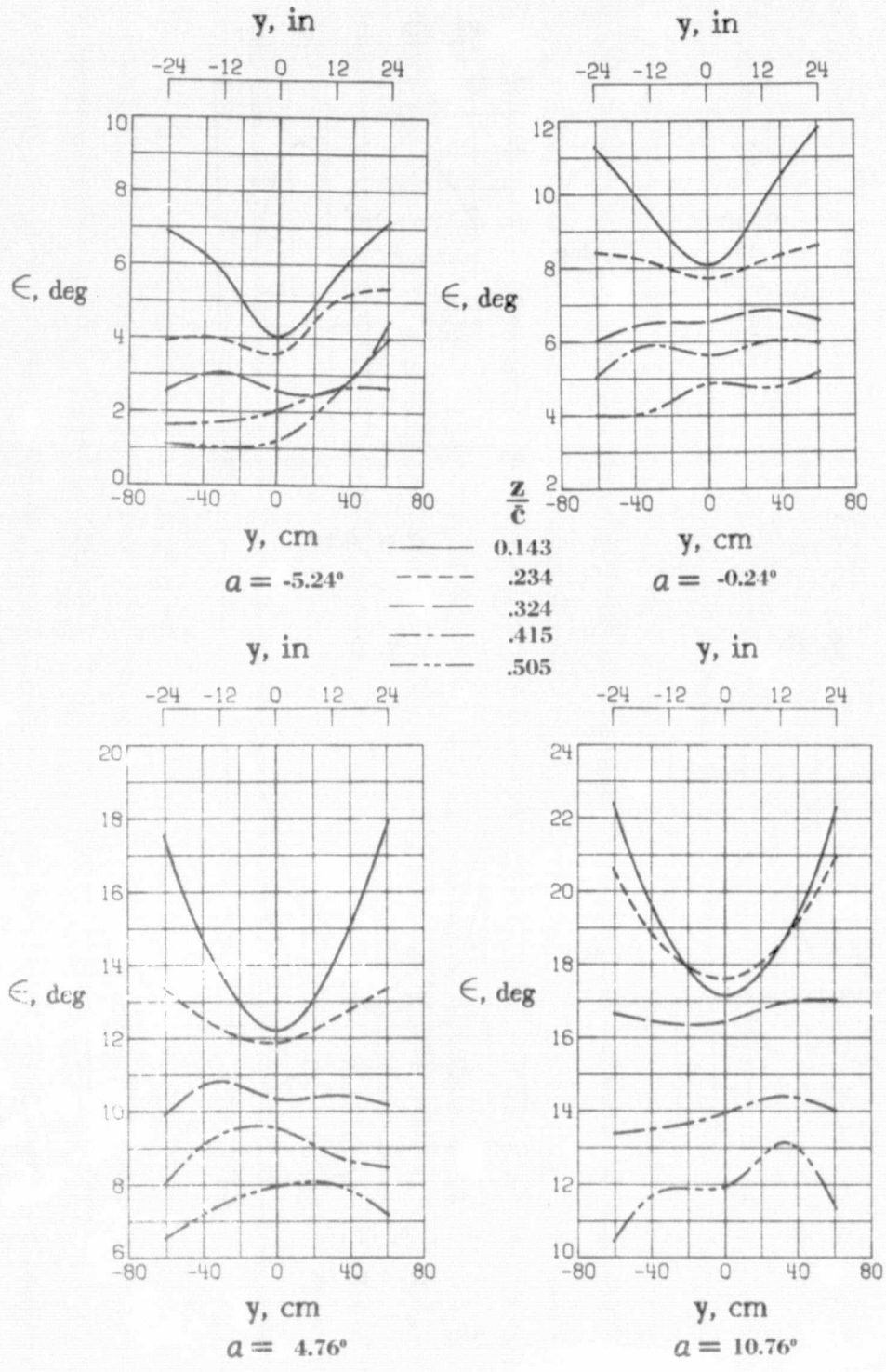

(a) $T_c' = 0.2$; $t/\bar{c} = 0.982$

Figure 14.- Variation of downwash angle with spanwise station. $\delta_f = 20°$. Deflectors on.

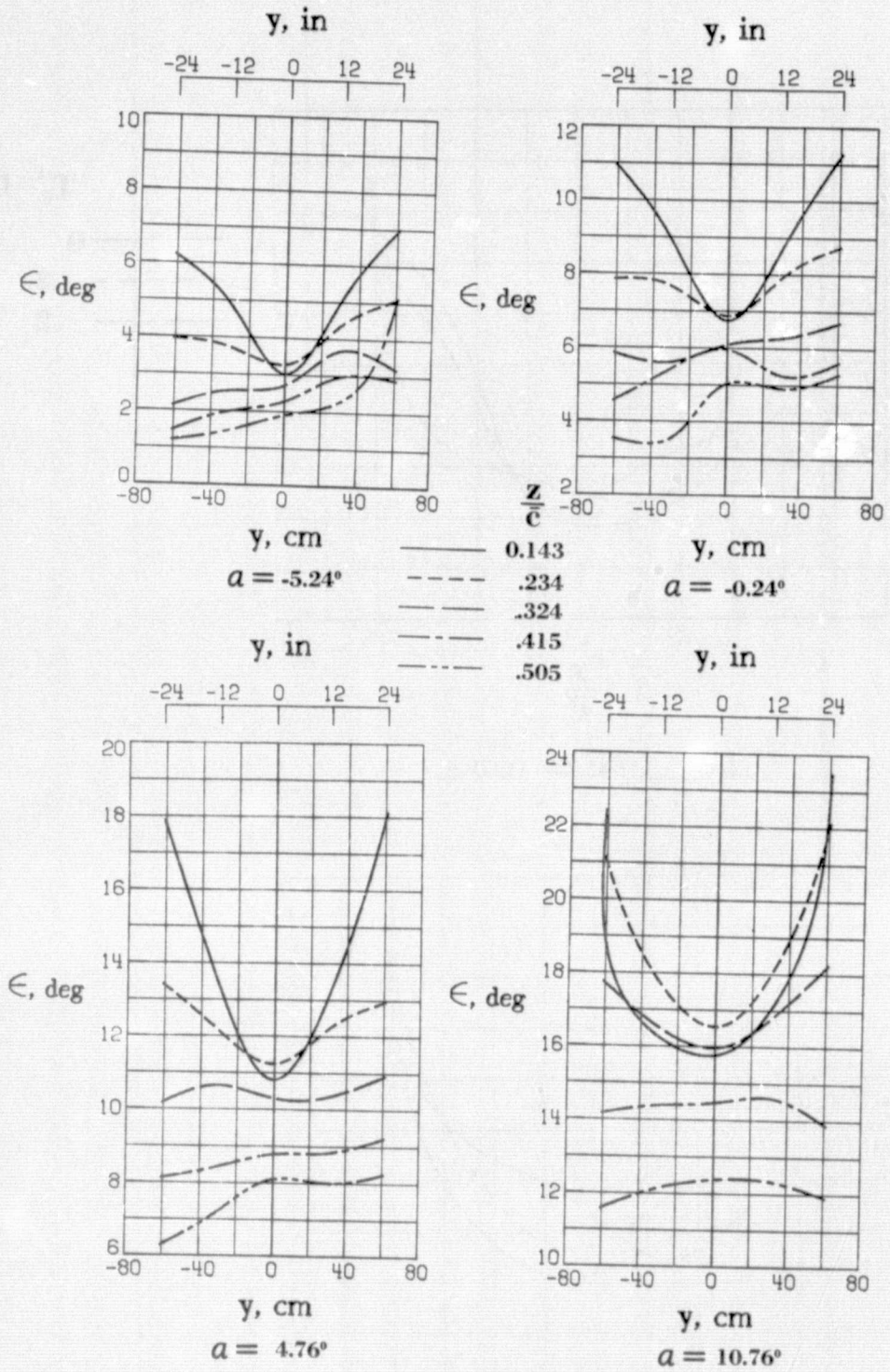

(b) $T_{\frac{c}{c}}^{l} = 0.20$; $t/\bar{c} = 1.254$.

Figure 14.- Concluded.

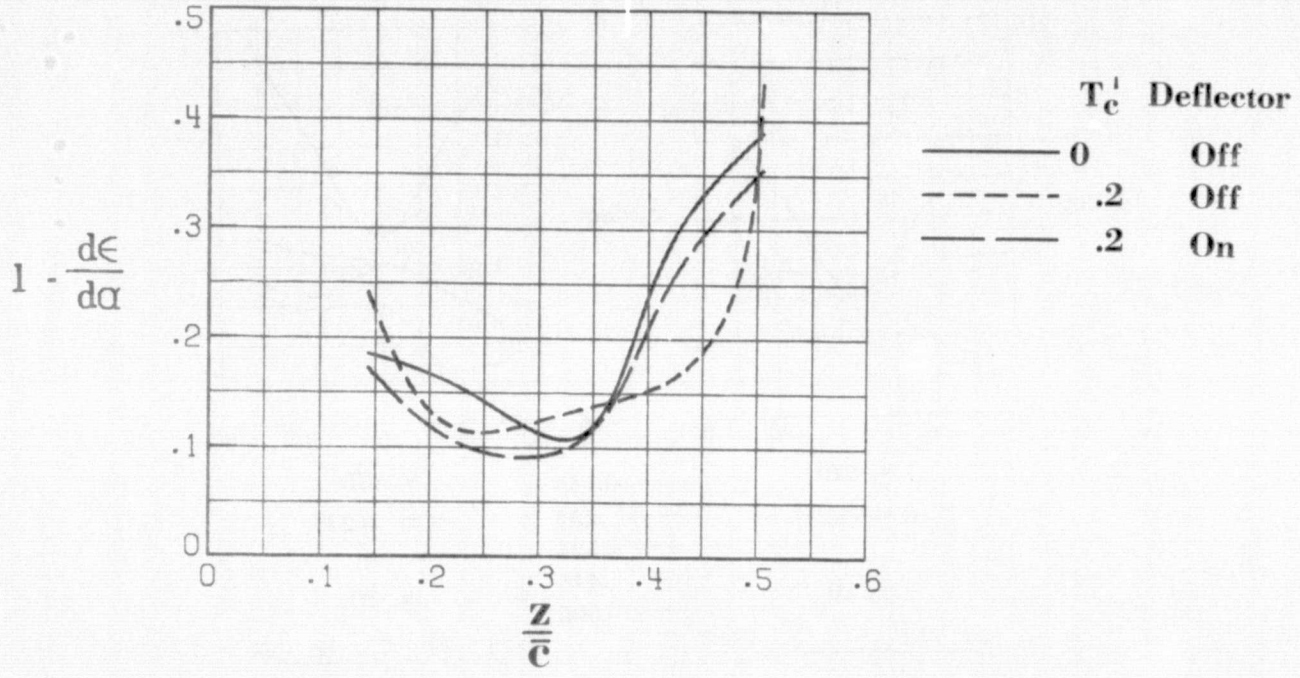

(a) $l / \bar{c} = 0.982.$

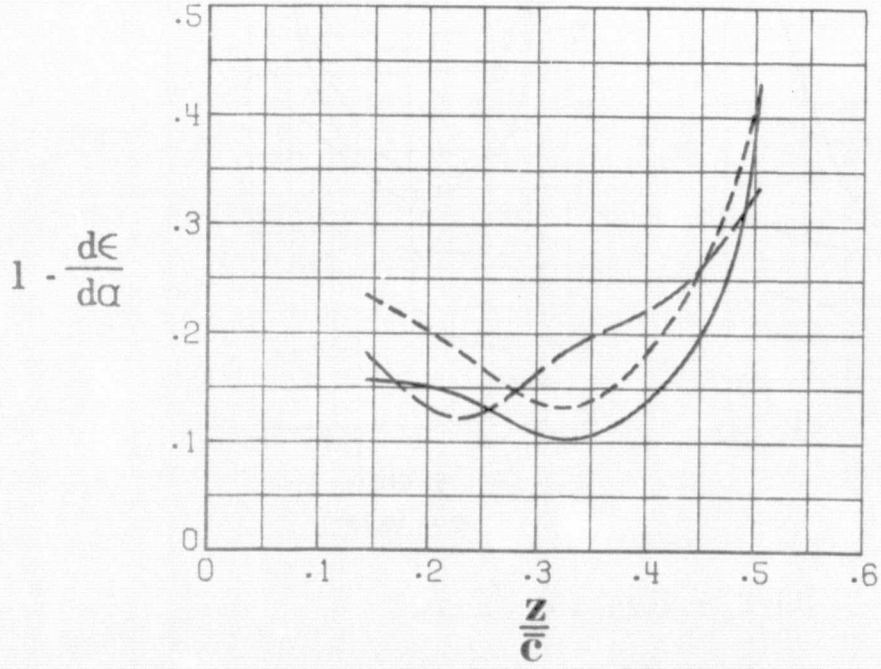

(b) $l / \bar{c} = 1.254.$

Figure 15.- Variation of downwash factor for various tail positions, tail heights, and thrust coefficients. $\delta_f = 20°$.

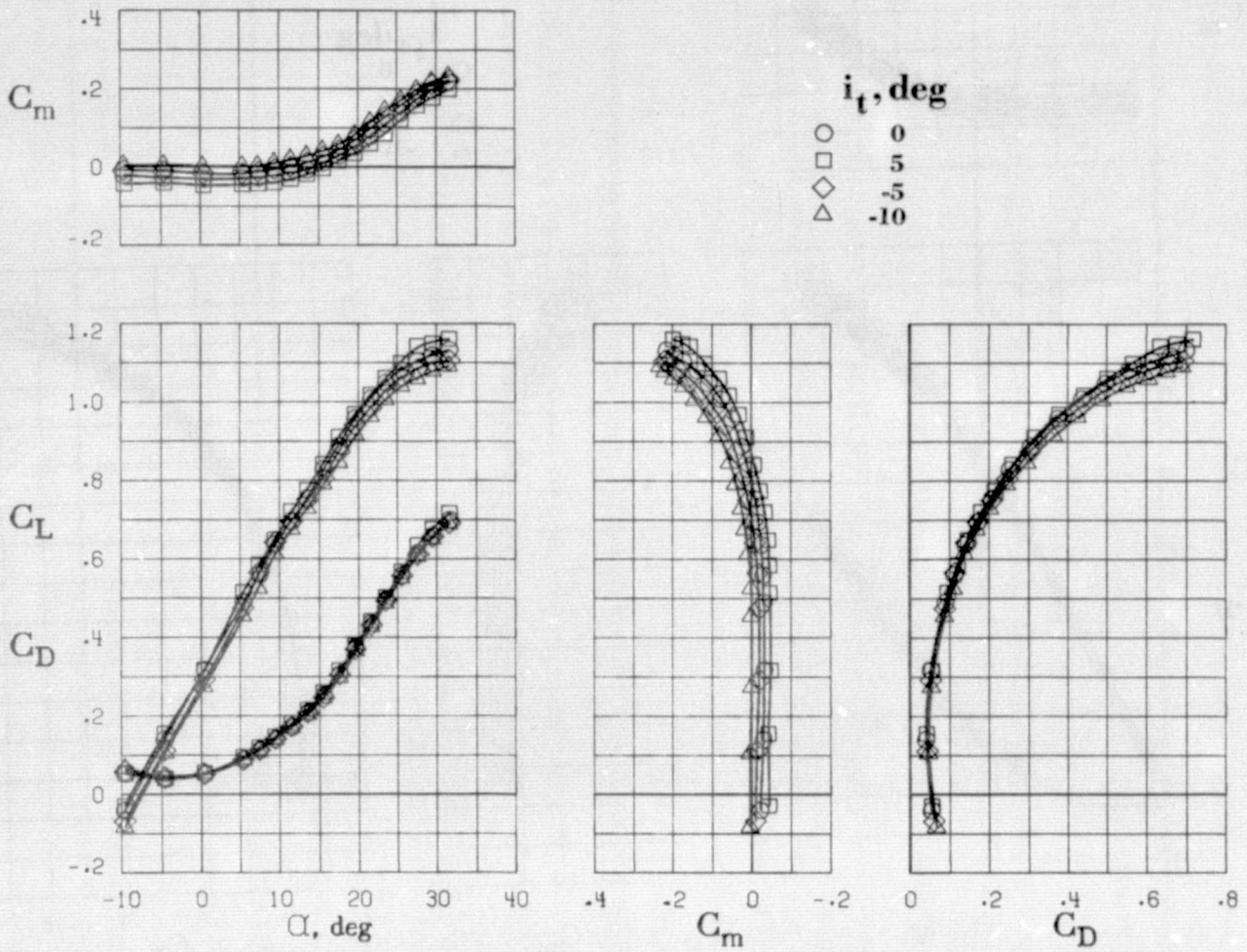

(a) $T_c' = 0^o$.

Figure 16.- Effect of tail incidence on the longitudinal aerodynamics characteristics for various thrust conditions. $\delta_f = 30^o$. 20° Exhaust deflectors installed. T-tail installed.

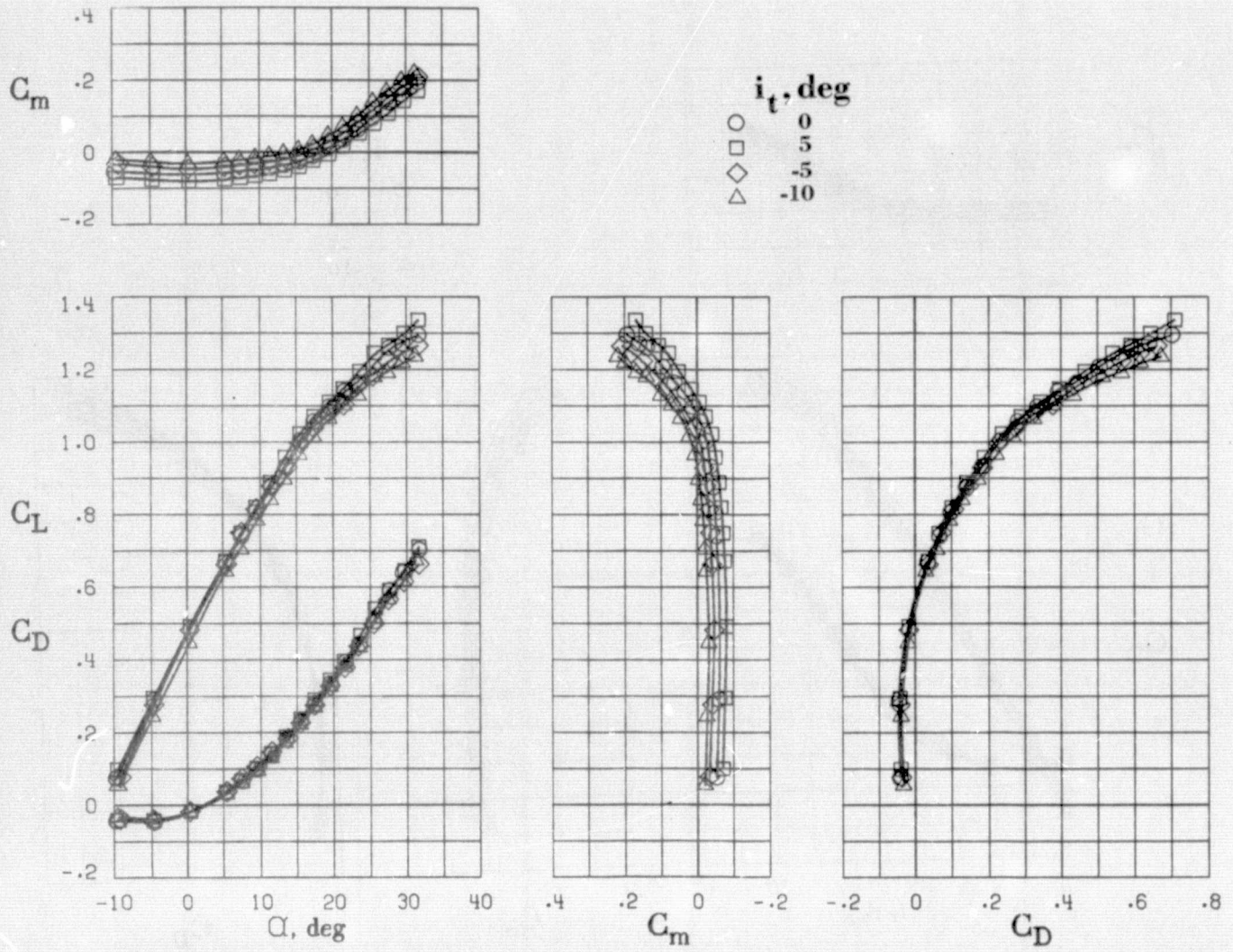

(b) $T_c' = 0.1$.

Figure 16.- Continued.

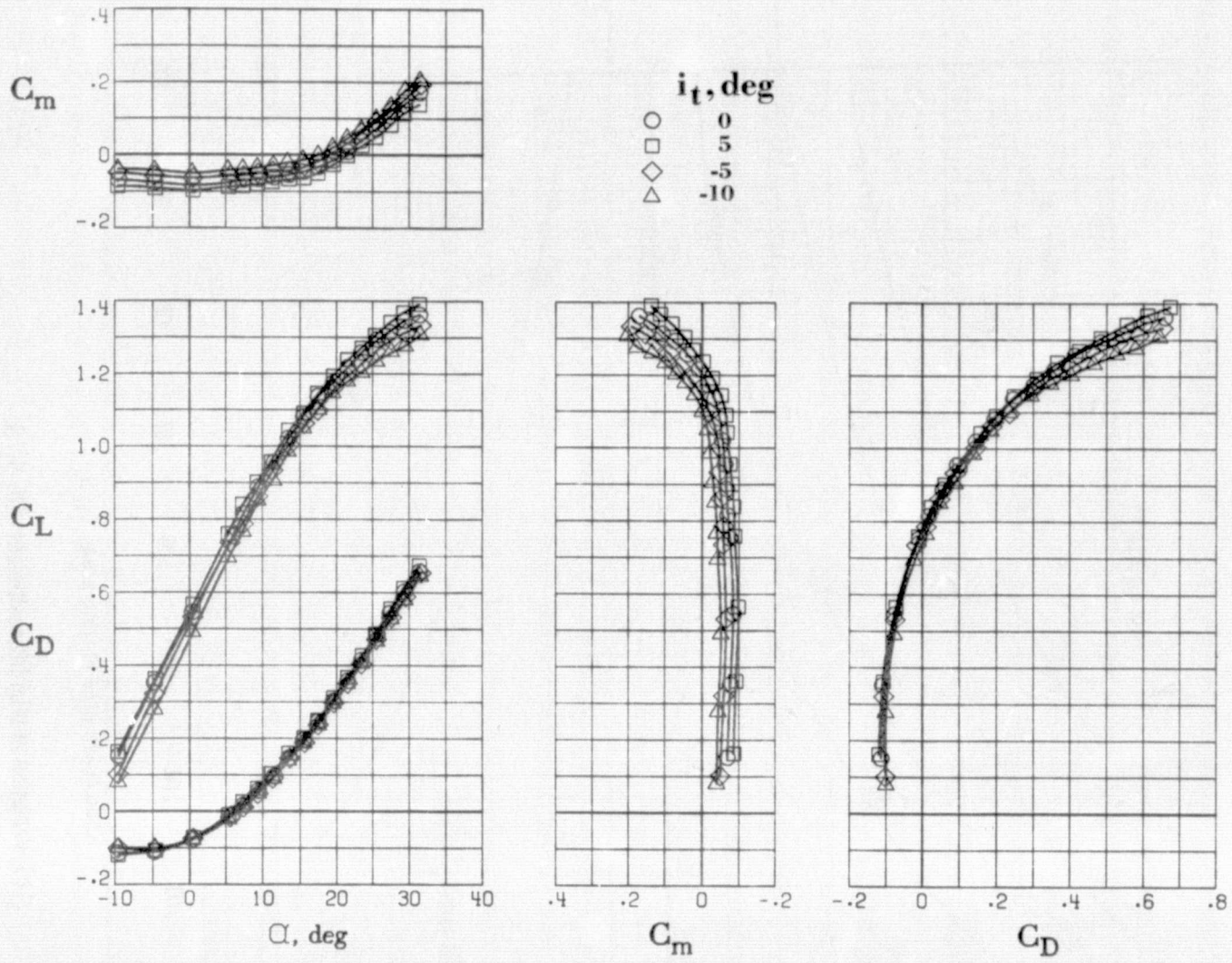

(c) $T_c' = 0.2$

Figure 16.- Concluded.

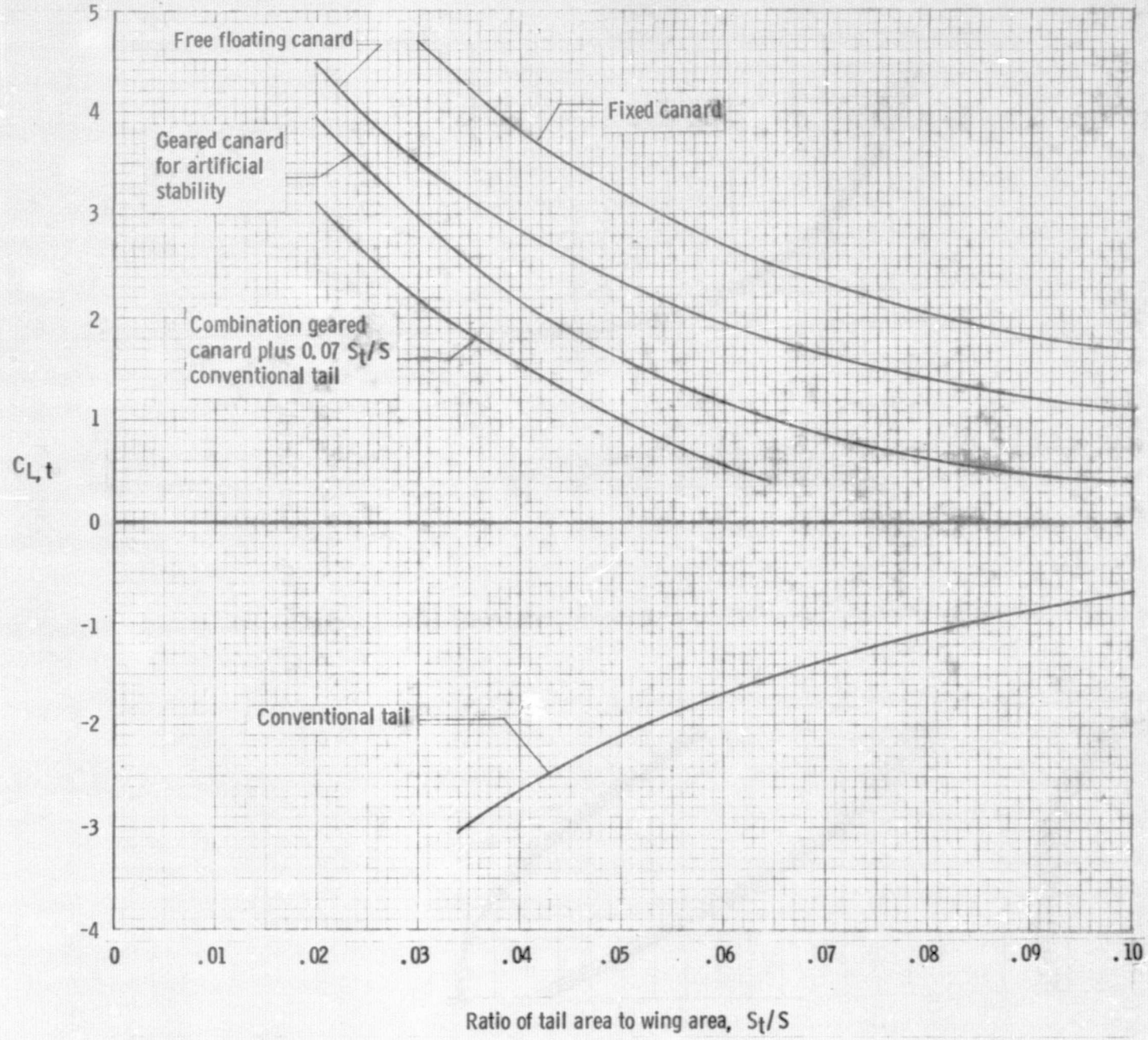

(a) Variation of trim lift coefficient with S_t/S.

Figure 17. - Comparison of several methods of achieving pitch trim and longitudinal stability. $\delta_f = 30°$.

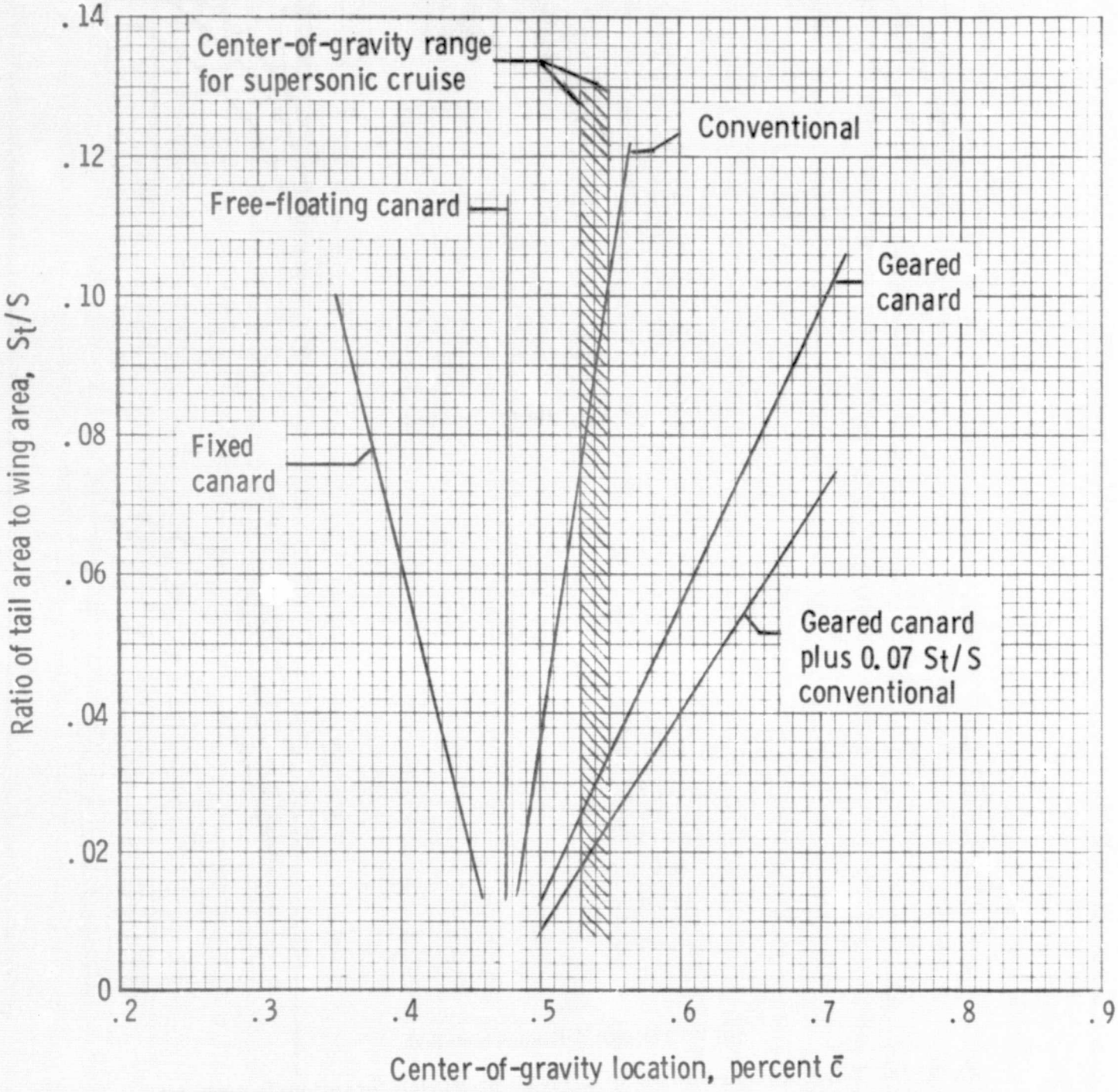

(b) Variation of center-of-gravity location with S_t/S.

Figure 17.- Concluded.

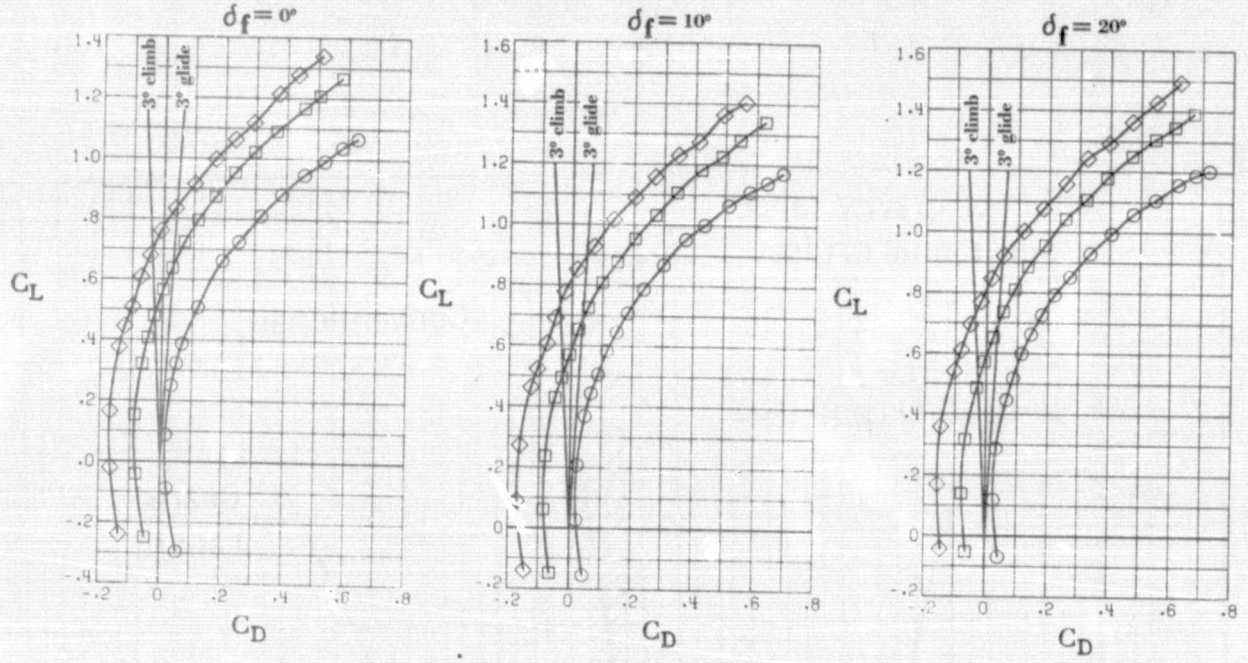

(a) No exhaust deflector installed.

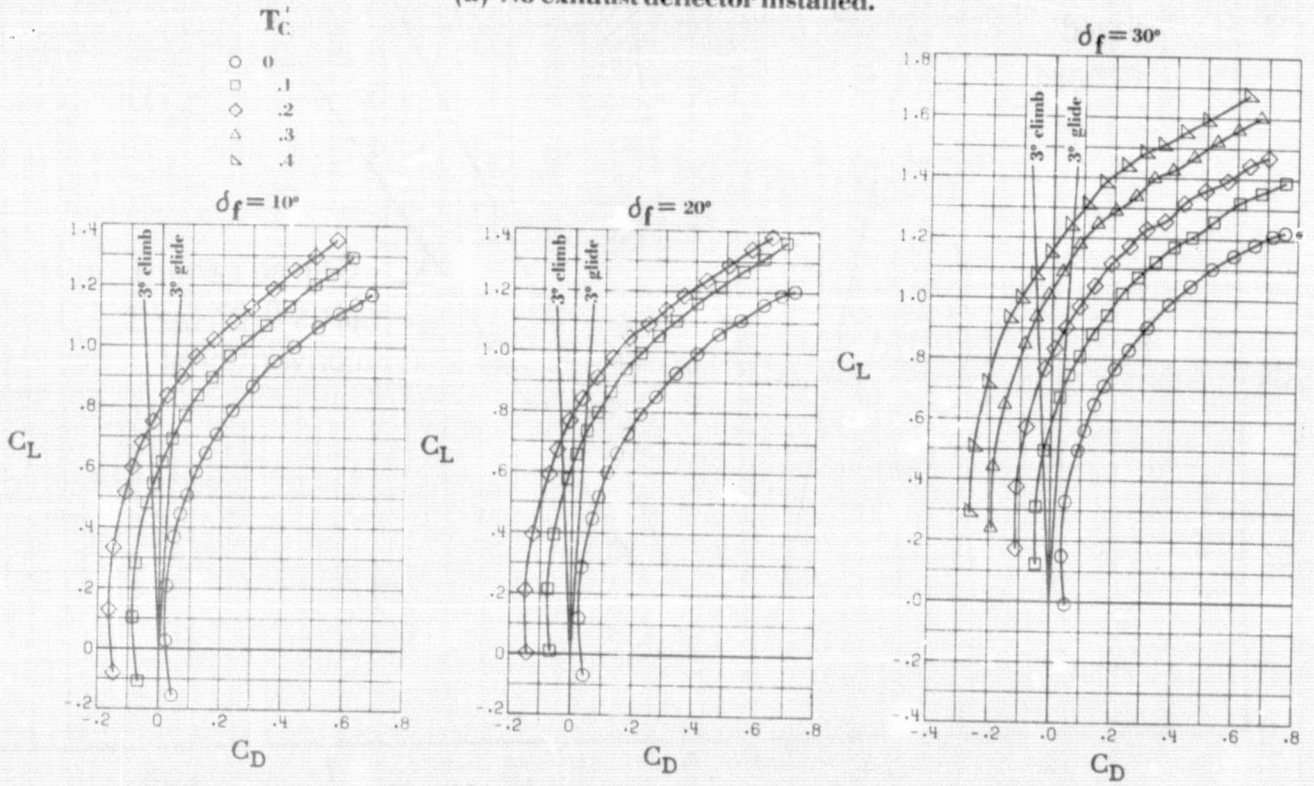

(b) 20° exhaust deflectors installed.

Figure 18.- Effect of exhaust deflectors on the lift-drag polars for various flap settings.

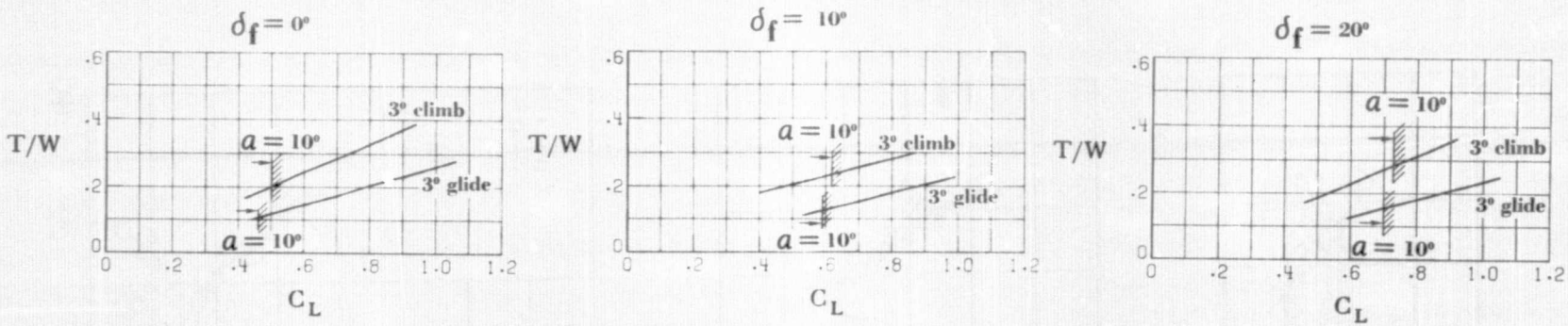

(a) No exhaust deflector installed.

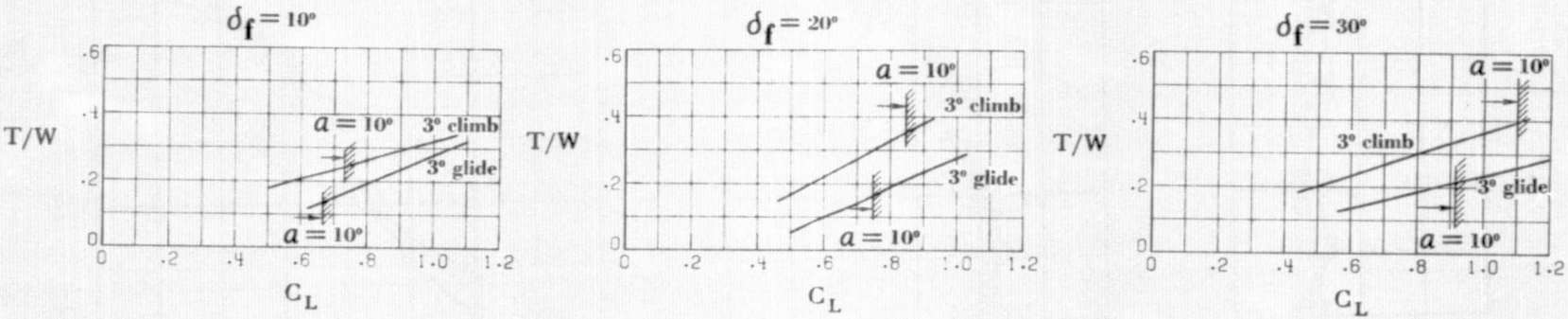

(b) 20° exhaust deflectors installed.

Figure 19.- Effect of exhaust deflectors on T/W vs C_L for various flap deflections.

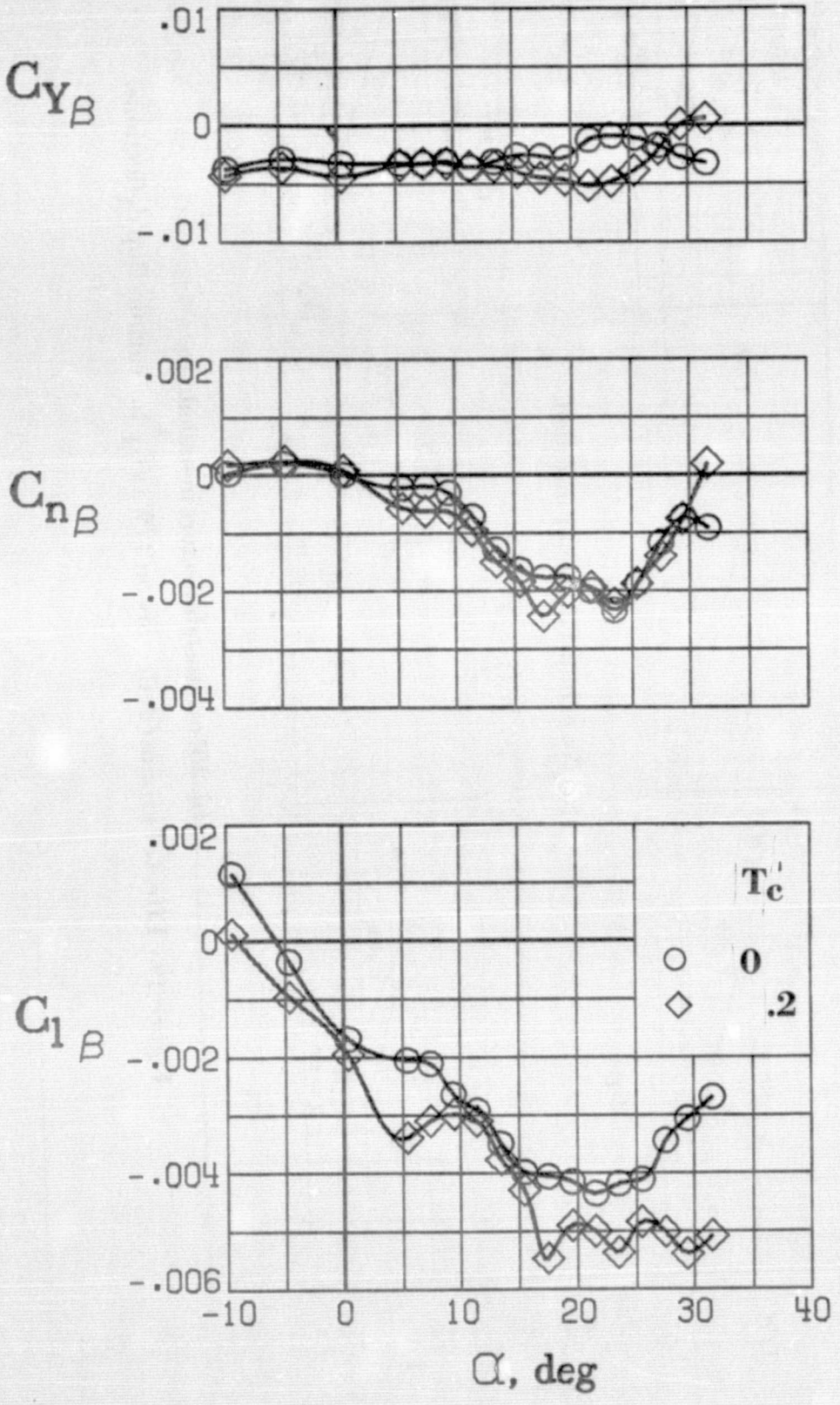

(a) Tail off.

Figure 20.- Effect of thrust coefficient on the static lateral-directional stability derivatives. 20° exhaust deflectors installed. $\delta_f = 30°$.

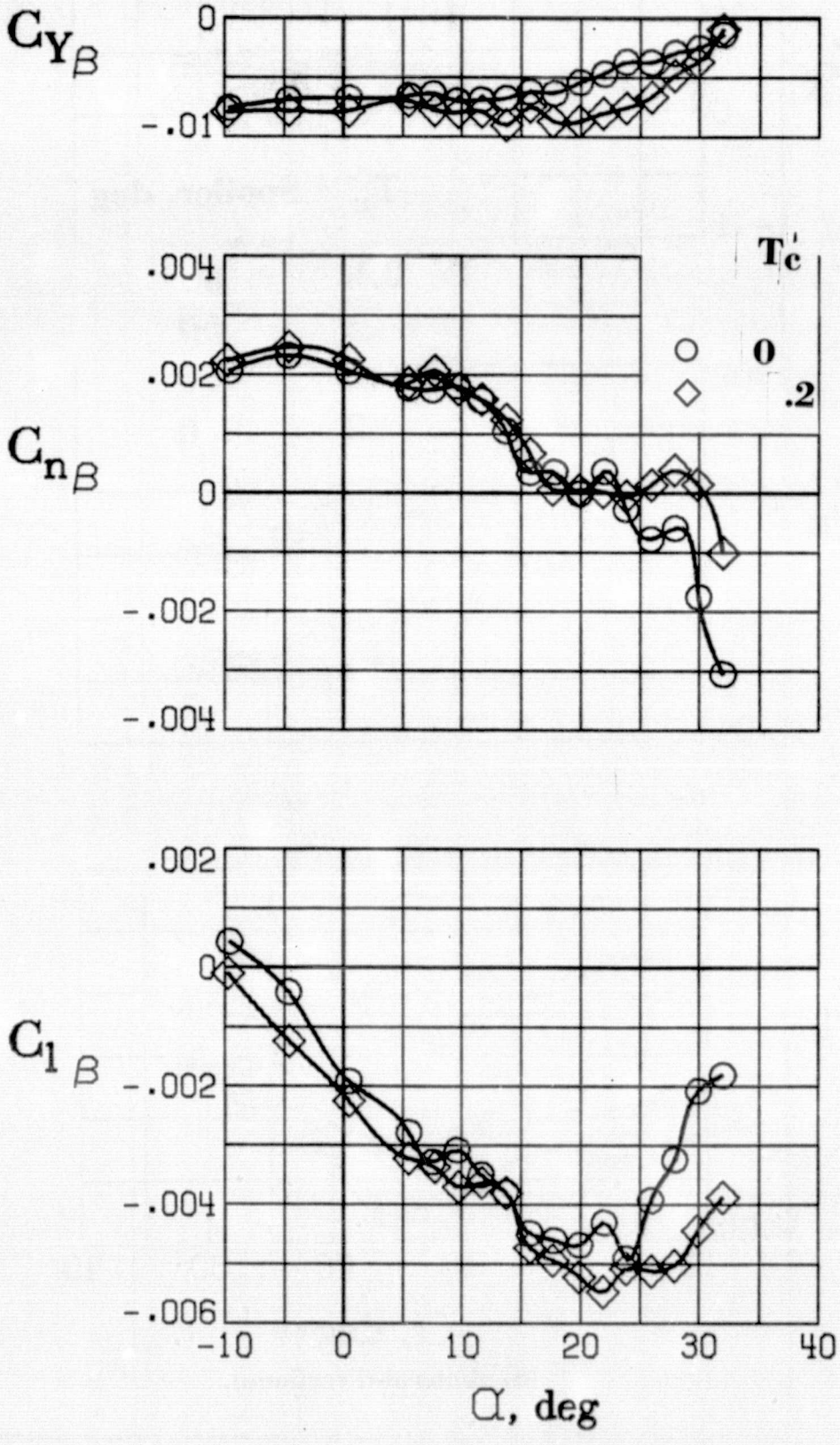

(b) Tail on.

Figure 20.- Concluded.

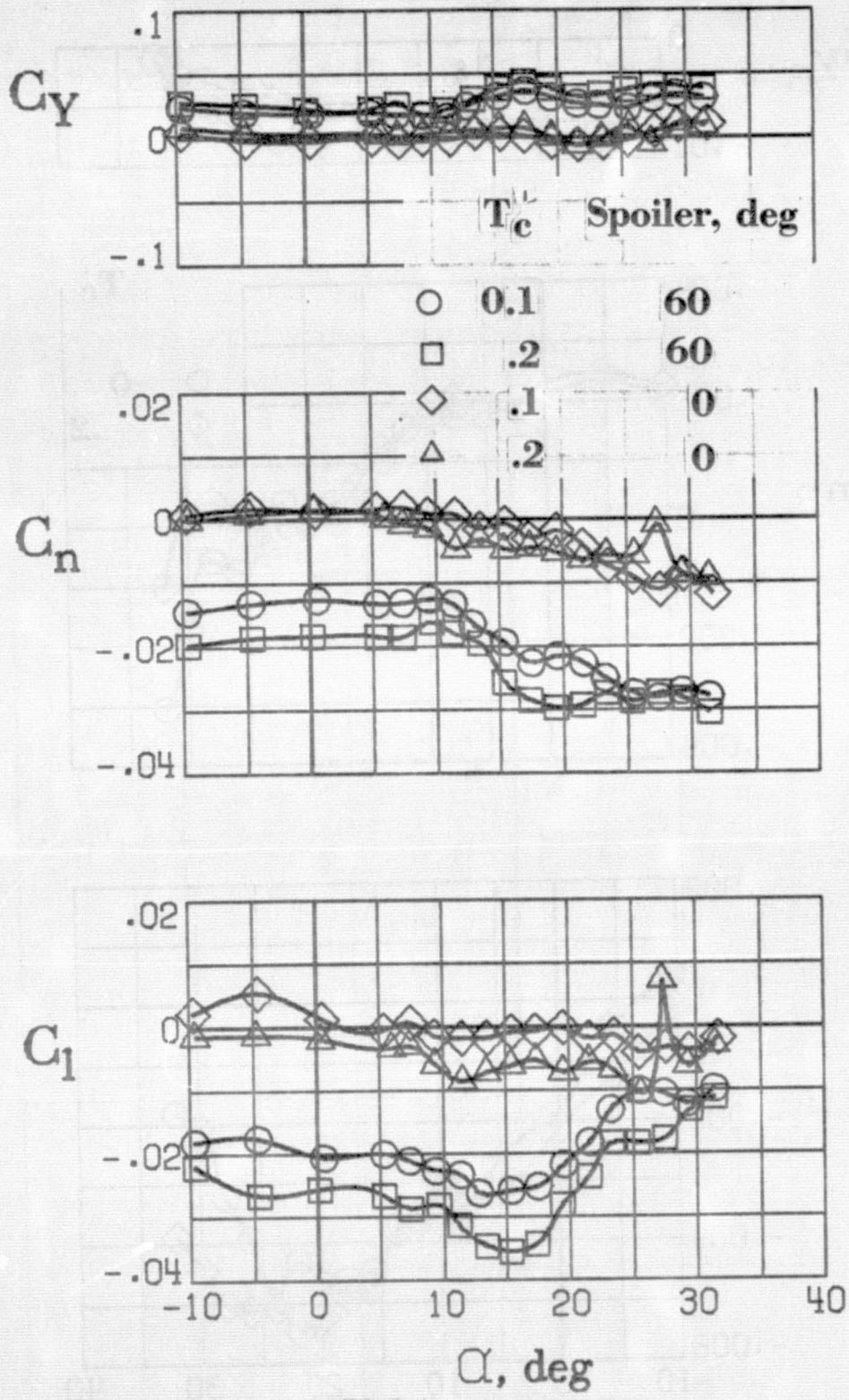

(a) Lateral-directional.

Figure 21.- Effect of spoilers on the static lateral and longitudinal aerodynamic characteristics for various thrust coefficients. 20° exhaust deflectors installed. $\delta_f = 30°$. T-tail on.

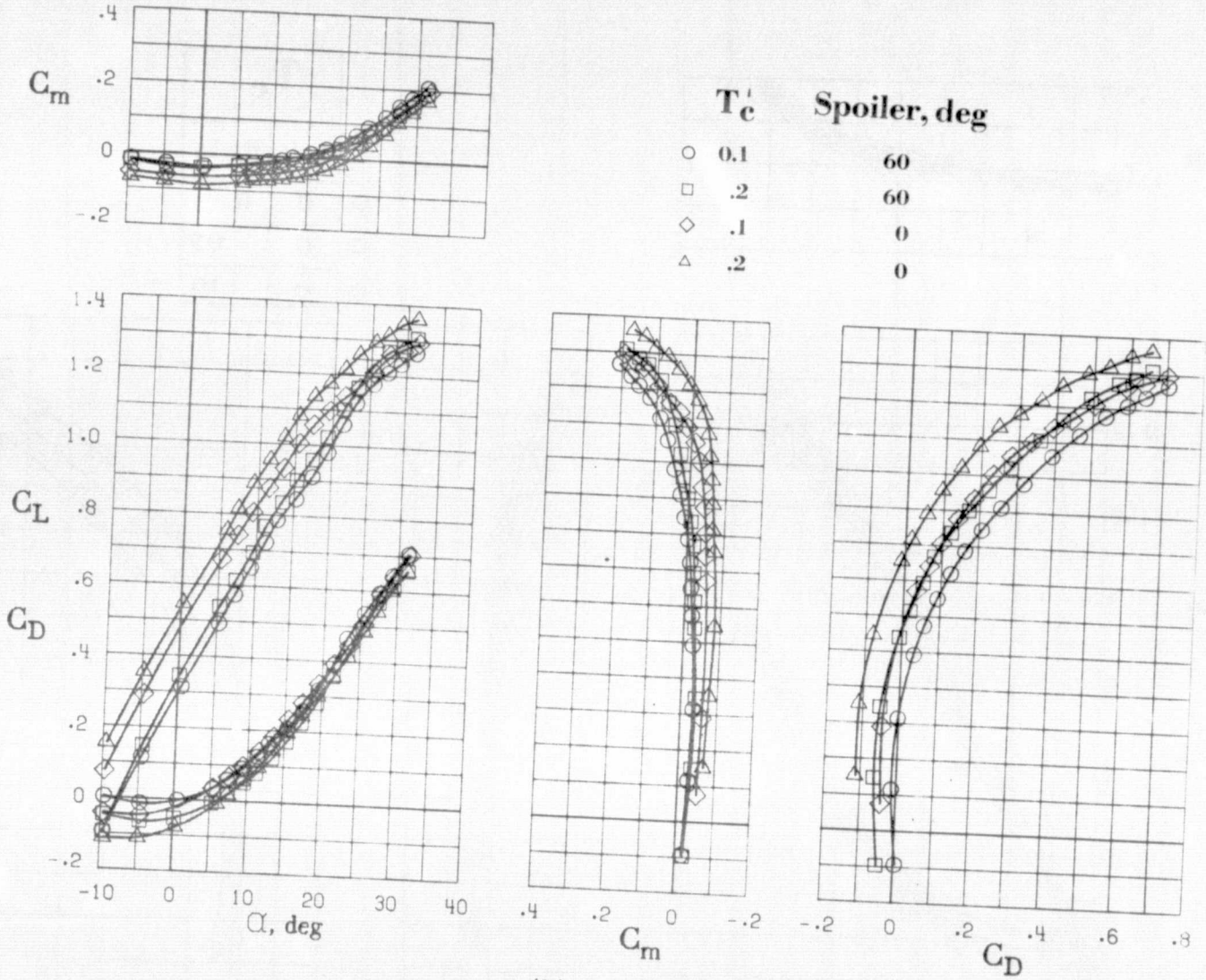

(b) Longitudinal.

Figure 21.- Concluded.

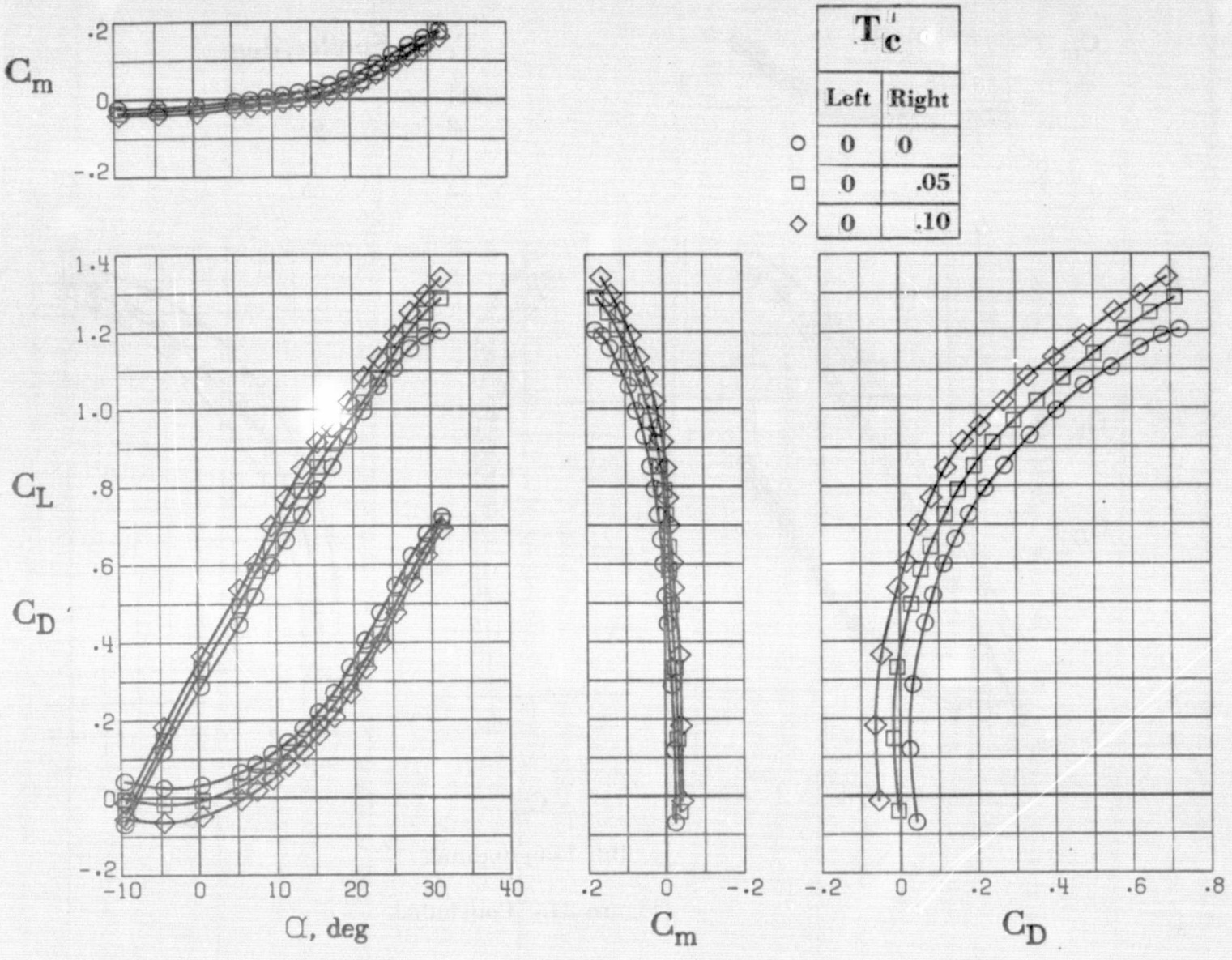

(b) Longitudinal.

Figure 22.- Concluded.

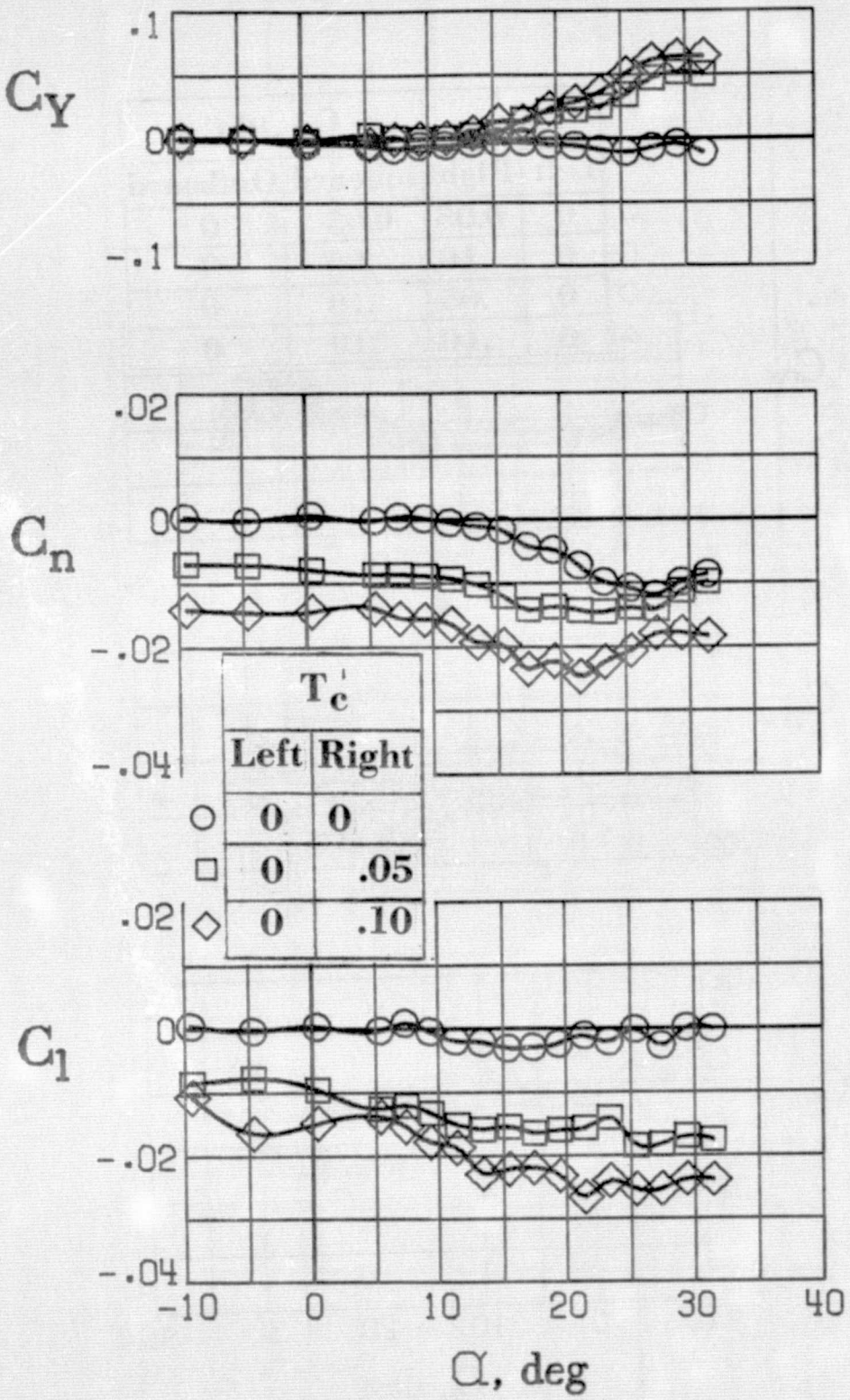

(a) Lateral-directional.

Figure 22.- Effect of one engine inoperative on the static lateral and longitudinal aerodynamic characteristics for various thrust coefficients. 20° exhaust deflectors installed $\delta_f = 20°$.

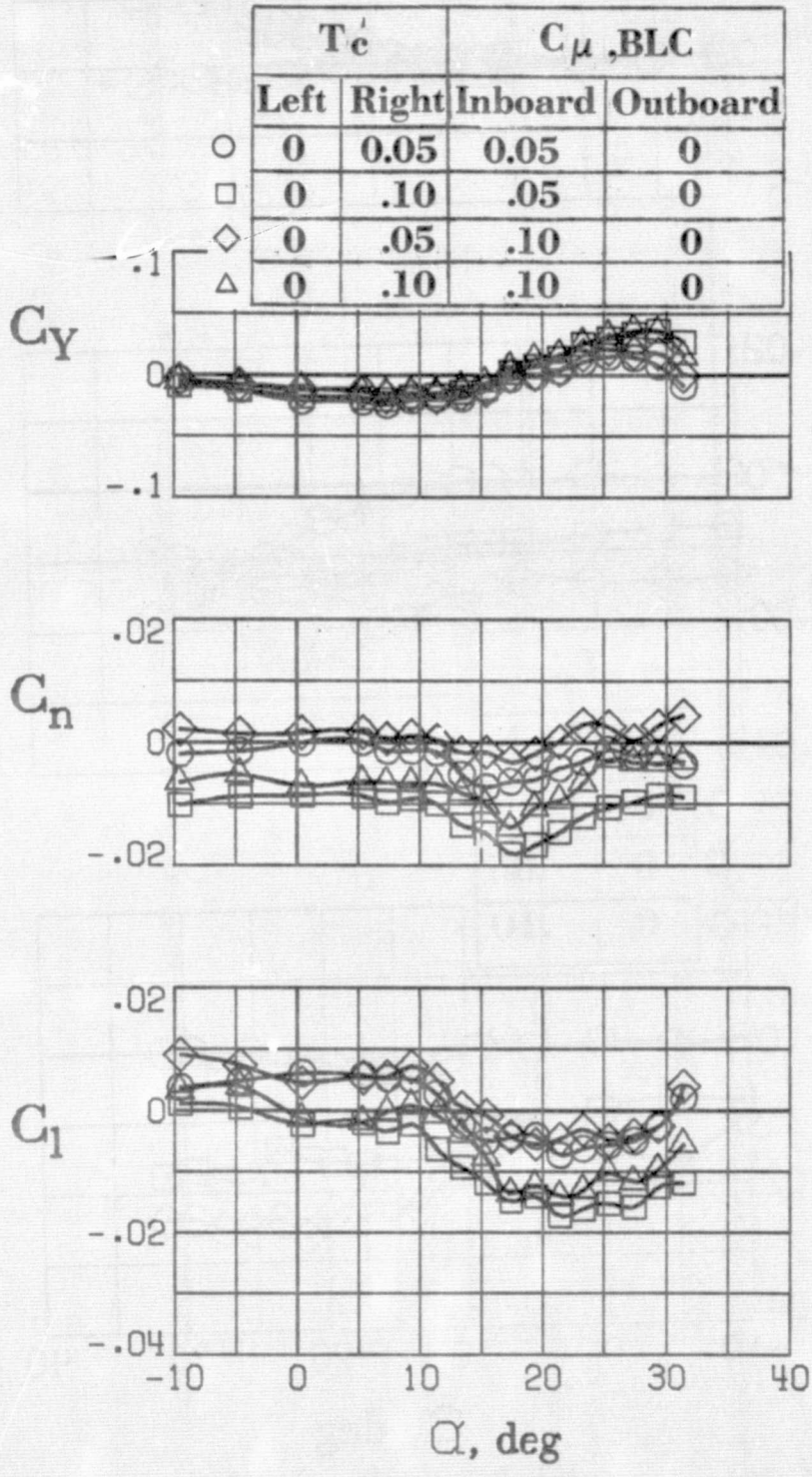

(a) Lateral-directional.

Figure 23.- Effect of asymmetric boundary layer control on the static lateral and longitudinal aerodynamic characteristics for various thrust and blowing coefficients. 20° exhaust deflectors installed. $\delta_f = 20°$.

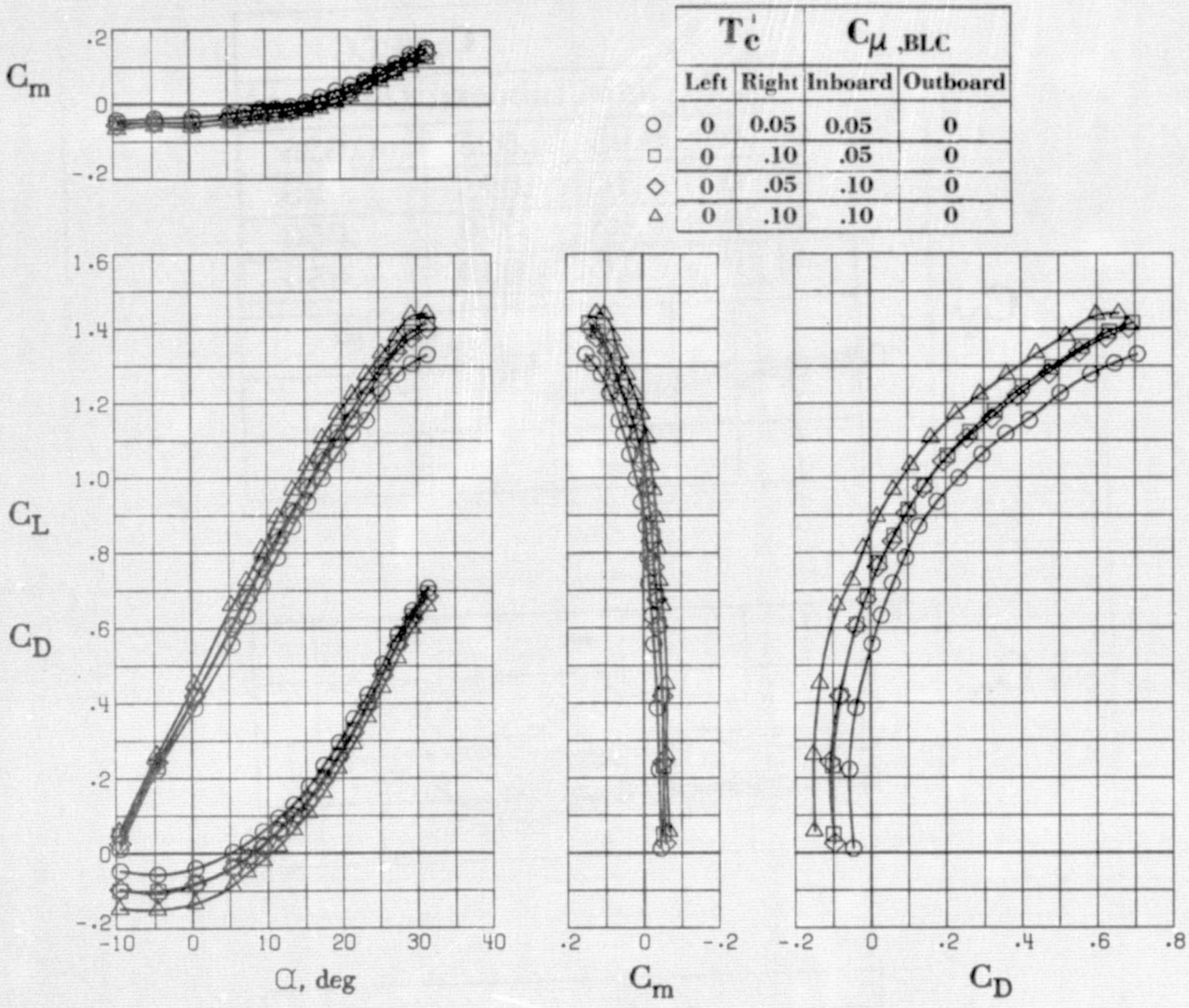

(b) Longitudinal.

Figure 23.- Concluded.

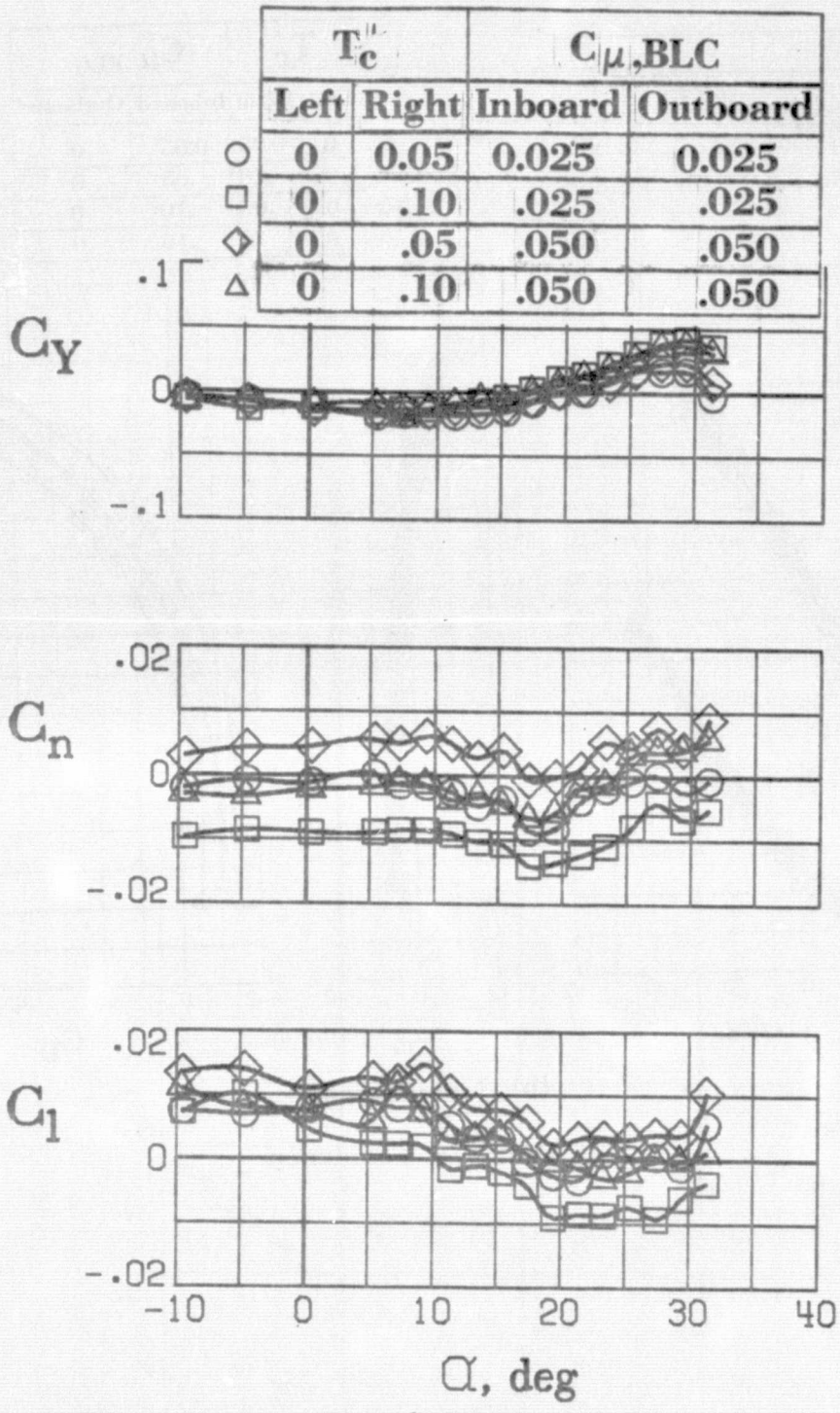

(a) Lateral-directional.

Figure 24.- Effect of asymmetric boundary layer control on the static lateral and longitudinal aerodynamic characteristics for various thrust and blowing coefficients. 20° exhaust deflectors installed. $\delta_f = 20°$.

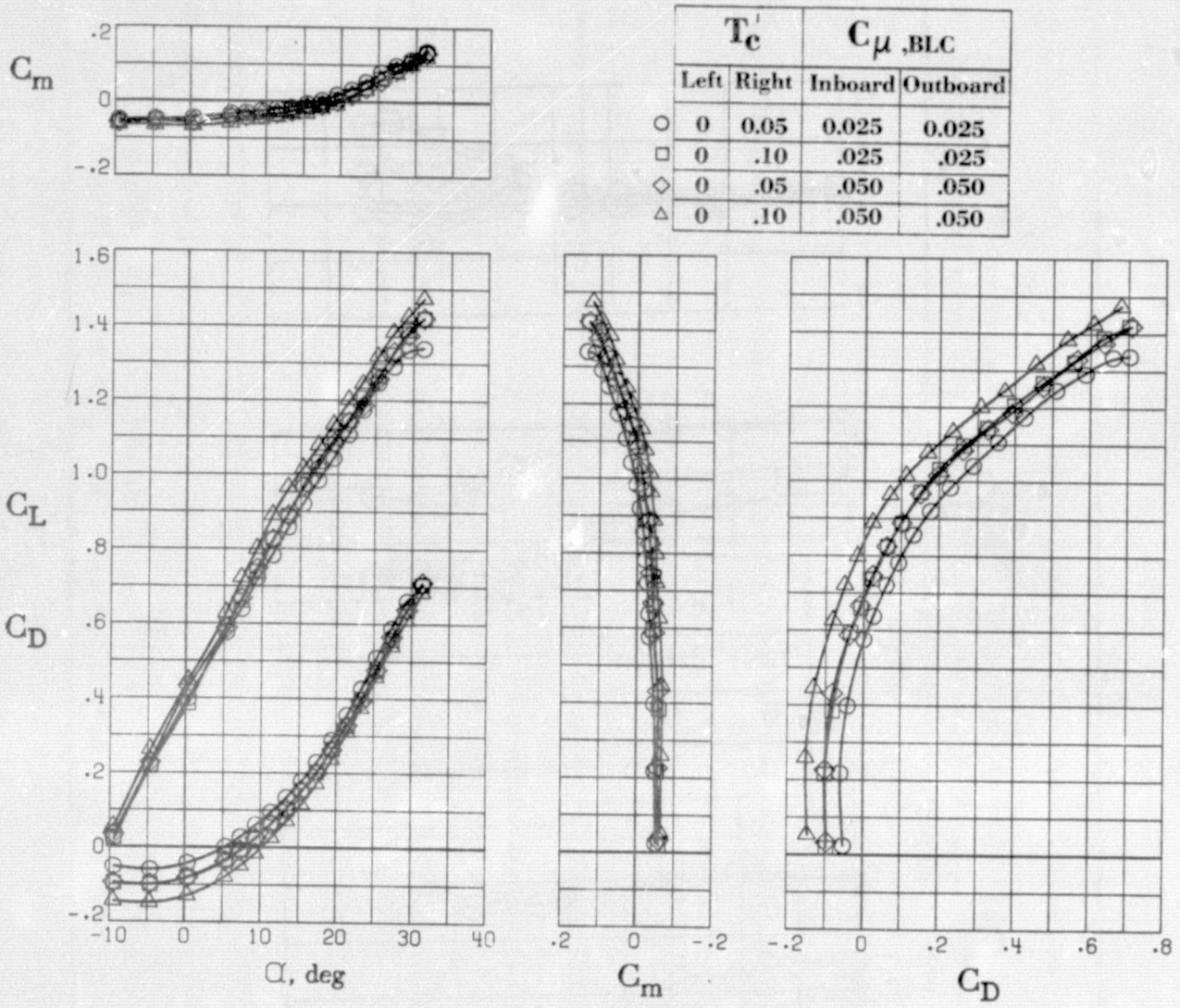

	T_c'		$C_{\mu,BLC}$	
	Left	Right	Inboard	Outboard
○	0	0.05	0.025	0.025
□	0	.10	.025	.025
◇	0	.05	.050	.050
△	0	.10	.050	.050

(b) Longitudinal.

Figure 24.- Concluded.

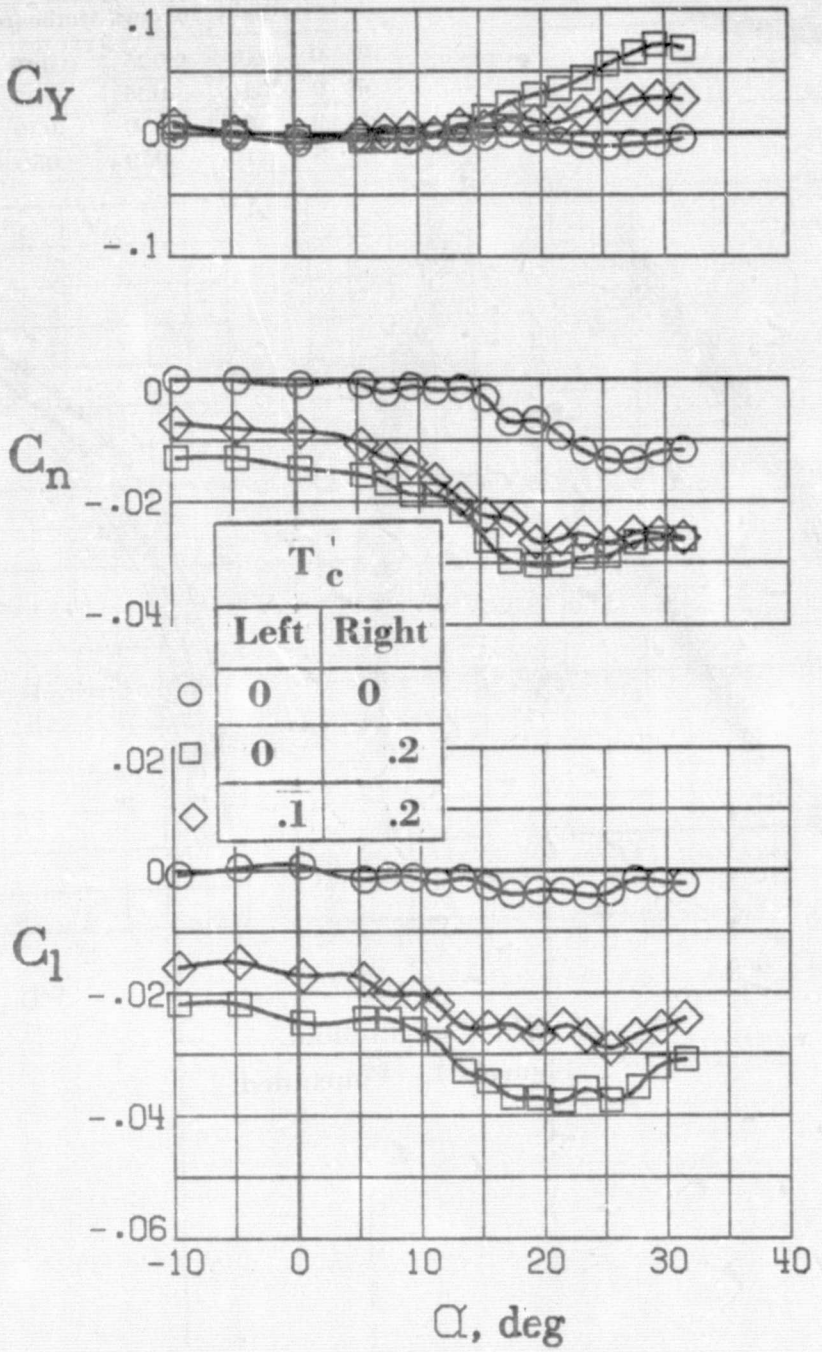

(a) Lateral-directional.

Figure 25.- Effect of asymmetric engine thrust coefficients on the static lateral and longitudinal aerodynamic characteristics. 20° exhaust deflectors installed. $\delta_f = 30°$.

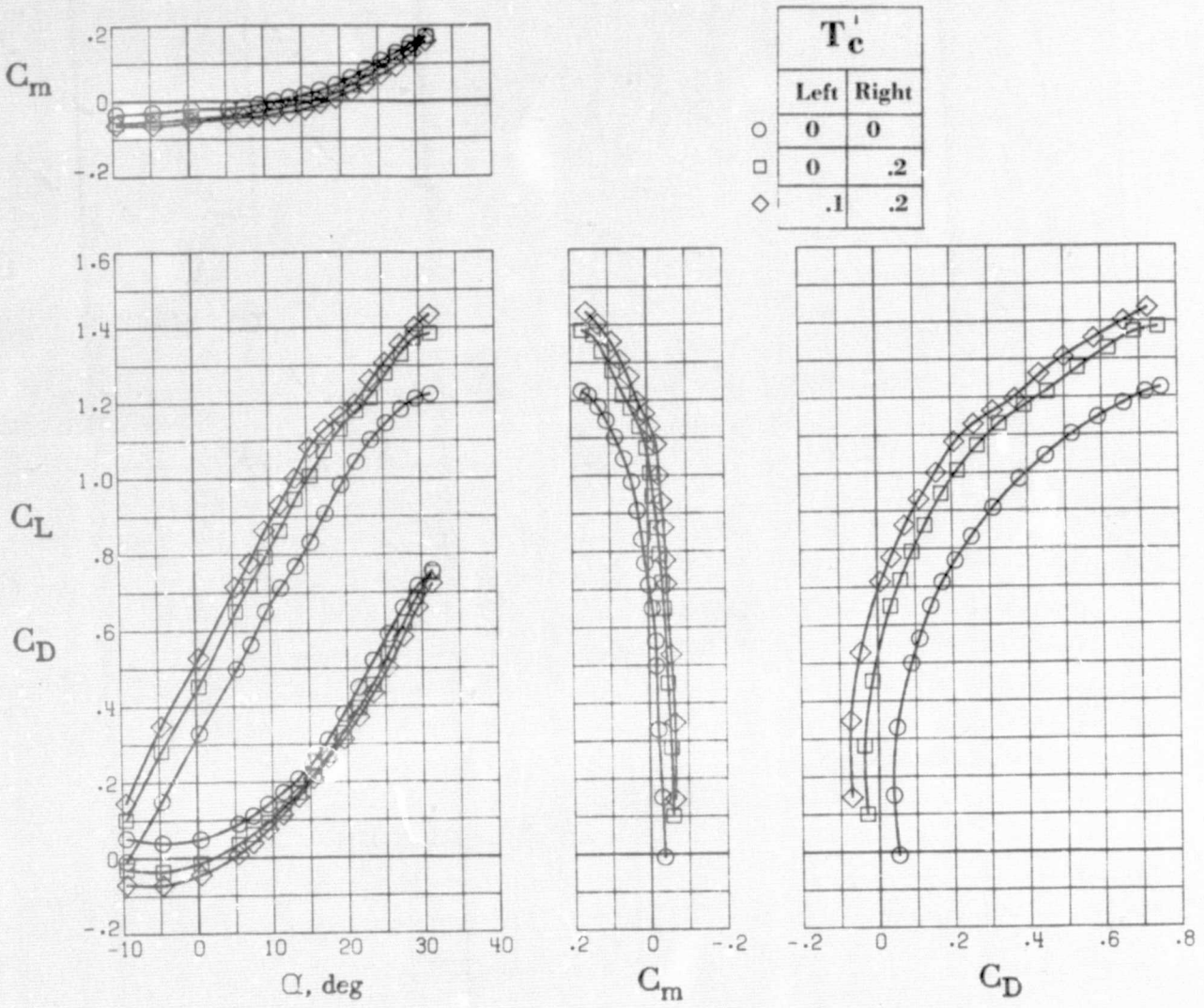

(b) Longitudinal.

Figure 25.- Concluded.